Strong coupling of single emitters to surface plasmons

D. E. Chang,[1] A. S. Sørensen,[2] P. R. Hemmer,[1,3] and M. D. Lukin[1,4]
[1]*Physics Department, Harvard University, Cambridge, Massachusetts 02138, USA*
[2]*Niels Bohr Institute, DK-2100 Copenhagen Ø, Denmark*
[3]*Electrical Engineering Department, Texas A&M University, College Station, Texas 77843, USA*
[4]*Harvard-Smithsonian Center for Astrophysics, ITAMP, Cambridge, Massachusetts 02138, USA*
(Received 24 March 2006; revised manuscript received 6 June 2007; published 18 July 2007)

We propose a method that enables strong, coherent coupling between individual optical emitters and electromagnetic excitations in conducting nanostructures. The excitations are optical plasmons that can be localized to subwavelength dimensions. Under realistic conditions, the tight confinement causes optical emission to be almost entirely directed into the propagating plasmon modes via a mechanism analogous to cavity quantum electrodynamics. We first illustrate this result for the case of a nanowire, before considering the optimized geometry of a nanotip. We describe an application of this technique involving efficient single-photon generation on demand, in which the plasmons are efficiently outcoupled to a dielectric waveguide. Finally, we analyze the effects of increased scattering due to surface roughness on these nanostructures.

DOI: 10.1103/PhysRevB.76.035420 PACS number(s): 73.20.Mf, 32.80.−t, 03.67.−a, 42.50.Pq

I. INTRODUCTION

In recent years, there has been substantial interest in nanoscale optical devices based on the electromagnetic surface modes (surface plasmons) associated with subwavelength metallic systems. Surface plasmons[1] are electromagnetic excitations associated with charge density waves on the surface of a conducting object. The unique properties of plasmons on nanoscale metallic systems have produced a number of dramatic observed effects, such as single molecule detection with surface-enhanced Raman scattering,[2,3] enhanced transmission through subwavelength apertures,[4,5] and enhanced photoluminescence from quantum wells.[6] There is also considerable interest in these systems in applications such as biosensing,[7] subwavelength imaging,[8,9] and waveguiding and switching devices below the diffraction limit.[10–13] Such subwavelength waveguiding of plasmons in metallic nanowires has been observed in a number of recent experiments.[14–16]

At the same time, spurred in part by rapid developments in the fields of quantum computation and quantum information science, there has been strong interest in exploring new physical mechanisms that enable coherent coupling between individual quantum systems and photon fields. Such a mechanism would enable quantum information to be passed over long distances and long-range interactions between systems. These features are not only essential for quantum communication[17,18] but would also facilitate the scalability of quantum computers.[19] The required coupling between emitters and photons is difficult but has been achieved in a number of systems that reach the so-called strong-coupling regime of cavity quantum electrodynamics (QED).[20–22] Recently, several approaches to reach this regime on a chip at microwave frequencies have been suggested[23–25] and experimentally observed,[22] which utilize coupling between emitters and modes of superconducting transmission lines. A key feature of these transmission lines is the reduction of the effective mode volume V_{eff} for the photons, which in turn results in a substantial increase of the emitter-field coupling constant $g \propto 1/\sqrt{V_{\mathrm{eff}}}$. Realization of analogous techniques with optical photons would open the door to many potential applications in quantum information science, and in addition, lead to smaller mode volumes and faster interaction times.

In this paper, we describe a method that enables strong, coherent coupling between individual emitters and electromagnetic excitations in conducting nanostructures on a chip at optical frequencies, via excitation of guided optical plasmons localized to nanoscale dimensions. The strong coupling occurs due to the subwavelength confinement and small mode volumes associated with the surface plasmon modes. We show that under realistic conditions optical emission can be almost entirely directed into these modes, in a manner similar to the Purcell effect in cavity QED. We first examine the case of a cylindrical nanowire, a simple geometry where the relevant physics can be understood analytically, before considering the more optimal geometry of a conducting nanotip. Defining a Purcell factor $P=\Gamma_{\mathrm{pl}}/\Gamma_{\mathrm{other}}$ characterizing the ratio of the spontaneous emission rate into the plasmon modes over emission into other channels, we show that values exceeding $P \sim 10^3$ are possible in these systems, limited only by metal losses at optical frequencies. Because of these losses, the plasmon modes themselves are not suitable as carriers of information over long distances. However, we show that the plasmon excitation can be efficiently converted into a photon in a nearby, evanescently coupled dielectric waveguide, as illustrated schematically in Fig. 1. This can be used, e.g, to create an efficient single-photon source or as part of an architecture to perform controlled interactions between distant qubits. The achievable coupling between the plasmon and waveguide systems can be much stronger than the plasmon dissipation rates, and we find that single-photon generation efficiencies exceeding 95% are possible for the simple geometries considered here.

This paper is organized as follows. In Sec. II, we calculate the mode structure of a conducting nanowire surrounded by some positive dielectric medium. We show that the nanowire supports one fundamental plasmon mode with significantly reduced phase velocity, which is tightly localized on a scale

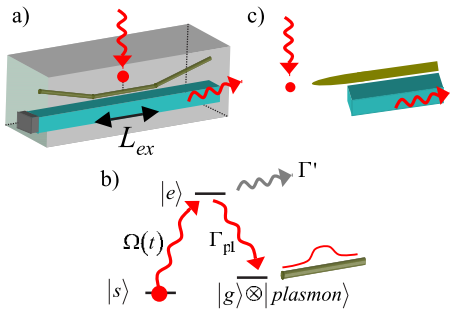

FIG. 1. (Color online) (a) An emitter coupled to a nanowire is optically excited and decays with high probability into the plasmon modes of the nanowire. A single-photon source is created by evanescently coupling the nanowire to a nearby dielectric waveguide over a length L_{ex}. The single-photon source can potentially be unidirectional, e.g., by capping one end of the waveguide with a reflective surface. (b) An internal-level scheme that allows for shaping of the outgoing single-photon pulses. An emitter that starts in state $|s\rangle$ is coupled to excited state $|e\rangle$ via a time-dependent external control field $\Omega(t)$. We assume that the excited state $|e\rangle$ is coupled to state $|g\rangle$ via the plasmon modes, causing $|e\rangle$ to decay into $|g\rangle$ with high probability, while simultaneously generating a single photon in the plasmon modes. The shape of the photon wave packet is determined by $\Omega(t)$. (c) A similar scheme for single-photon generation using an emitter coupled to a nanotip instead of a nanowire. Note that this scheme is naturally unidirectional, as the generated plasmons propagate in a single direction.

$\sim R$ around the wire surface. We also calculate the dissipation rate of the fundamental mode as it propagates along the nanowire, due to metallic losses. In Sec. III, we calculate the emission properties of a dipole emitter near the nanowire as a function of emitter position and wire radius. We show that under certain circumstances, emission into the guided plasmon modes is greatly enhanced over decay into radiative and nonradiative channels. In fact, when optimized, the probability of emission into the plasmon mode approaches almost unity for small R and is limited only by inherent losses in the metal. While the nanowire is a simple system to understand, we note that there is an inherent trade-off present in this geometry, as the small wire sizes that yield strong coupling also result in more rapid dissipation of the plasmons as they propagate. Therefore, in Sec. IV, we consider a better-optimized system, a conducting nanotip. We show that the nanotip can significantly reduce the effects of propagative losses even while preserving large coupling strengths. In Sec. V, we consider the problem of outcoupling the plasmon modes, and study in detail the interaction between the plasmon modes of our nanostructures and the guided modes of a nearby dielectric waveguide. We show that the plasmon modes can be efficiently outcoupled to the waveguide, and we propose an architecture for efficient single-photon generation on demand based on a tiered emitter/nanostructure/waveguide system. We calculate the expected efficiencies for single-photon generation, taking fully into account the propagative losses of the plasmons, the finite Purcell factors governing the interactions with the dipole emitter, and the nonunity coupling efficiency between the plasmon and waveguide modes. In Sec. VI, we consider the effects of possible imperfections to the system, in particular, the adverse effect of surface roughness on the conducting nanostructures. In general, surface roughness can lead to radiative scattering of plasmons as well as increased nonradiative dissipation, which results in larger losses as the plasmons propagate along the structure. We calculate the effects of these two processes and find only moderate increases in the total loss under reasonable parameters. Finally, in Sec. VII, we summarize our results while outlining possible physical realizations and discussing some future directions of research in this area.

II. PLASMON MODES ON A NANOWIRE

The method for calculating the electromagnetic modes of a nanowire is briefly outlined here, with details of the calculation given in Appendix A. We consider a cylinder of radius R of dimensionless electric permittivity ϵ_2, which is centered along the z axis and surrounded by a second dielectric medium ϵ_1. While we are particularly interested in the case of a conducting nanowire surrounded by some lossless positive dielectric ($\mathrm{Re}\,\epsilon_2<0, \epsilon_1>0$), we note that at this point the discussion is quite general. Like any other simple geometry with a high degree of symmetry, one can use separation of variables and find field solutions $\mathbf{E}$, $\mathbf{H}$ to Maxwell's equations in each dielectric region.[26,27] In cylindrical coordinates, the electric field is given by $\mathbf{E}_i(\mathbf{r})=\mathcal{E}_{i,m}\mathbf{E}_{i,m}(k_{i\perp}\rho)e^{im\phi}e^{ik_\parallel z}$, where $i=1,2$ denote the regions outside and inside the cylinder, respectively. Here, $k_\parallel$ is the longitudinal component of the wave vector, which is related to the vacuum wave vector $k_0=\omega/c$, electric permittivity ϵ_i, and transverse wave vector $k_{i\perp}$ by $\epsilon_i k_0^2=k_\parallel^2+k_{i\perp}^2$, and m is an integer characterizing the winding of the mode. The functions $\mathbf{E}_{i,m}$ represent some normalized mode profiles. A similar expression holds for the magnetic field $\mathbf{H}$. For future reference, we also define the vacuum wavelength $\lambda_0=2\pi/k_0$, and $k_i=\sqrt{\epsilon_i}k_0$ as the wave vector in medium i. The coefficients $\mathcal{E}_{i,m}$ and $\mathcal{H}_{i,m}$ multiplying the fields are not arbitrary but, instead, must satisfy a set of equations that enforces the necessary boundary conditions at the dielectric interface $\rho=R$. The existence of a nontrivial solution requires that the matrix corresponding to this linear system have zero determinant ($\det M=0$), which upon simplifying yields the mode equation,[26,27]

$$\frac{m^2k_\parallel^2}{R^2}\left(\frac{1}{k_{2\perp}^2}-\frac{1}{k_{1\perp}^2}\right)^2=\left[\frac{1}{k_{2\perp}}\frac{J_m'(k_{2\perp}R)}{J_m(k_{2\perp}R)}-\frac{1}{k_{1\perp}}\frac{H_m'(k_{1\perp}R)}{H_m(k_{1\perp}R)}\right]\times\left[\frac{k_2^2}{k_{2\perp}}\frac{J_m'(k_{2\perp}R)}{J_m(k_{2\perp}R)}-\frac{k_1^2}{k_{1\perp}}\frac{H_m'(k_{1\perp}R)}{H_m(k_{1\perp}R)}\right]. \tag{1}$$

The above equation, for example, determines the allowed values of $k_\parallel$ as functions of m, R, and ϵ_i.

We now focus on the case of a subwavelength, conducting metal wire surrounded by a normal, positive dielectric. In Fig. 2, we plot the allowed wave vectors $k_\parallel$, as determined through Eq. (1), as a function of R for a few lowest-order modes in m. For concreteness, all numerical results presented in this paper are for a silver nanowire (or later, nanotip) at

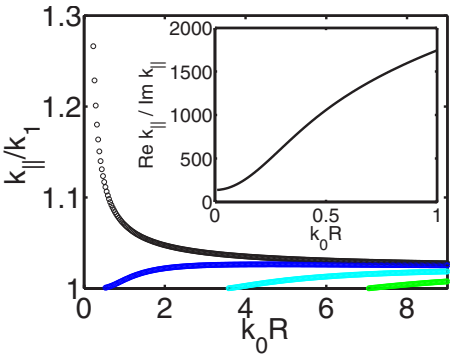

FIG. 2. (Color online) Allowed plasmon modes $k_{\|}$ as a function of R for a silver nanowire embedded in a surrounding dielectric $\epsilon_1=2$, for frequency corresponding to a vacuum wavelength $\lambda_0=1$ μm and room temperature. The fundamental ($m=0$) mode, in black, exhibits a $k_{\|}\propto 1/R$ dependence, while all other modes are effectively cut off as $R\to 0$. In order of increasing cutoff radius, the other modes displayed correspond to $|m|=1$, 2, and 3, respectively. Inset: the propagative losses for the fundamental mode, characterized by the ratio Re $k_{\|}$/Im $k_{\|}$, for the same parameters.

room temperature, $\lambda_0=1$ μm, and with a surrounding dielectric $\epsilon_1=2$, although the physical processes described are not specific to silver or to some narrow frequency range. The electric permittivity of the silver nanowire at this frequency is assumed to correspond to its measured value in thin films, $\epsilon_2\approx -50+0.6i$.[28,29] In plotting Fig. 2, we have temporarily ignored the dissipative imaginary part of ϵ_2, although we will address its effect later. Ignoring Im ϵ_2 results in purely real values of $k_{\|}$, indicating that these modes propagate without loss.

We first qualitatively discuss the important features of the plasmon modes illustrated in Fig. 2 before deriving them more carefully. It is clear from the figure that the longitudinal component of the wave vector exceeds the wave vector in uniform dielectric, $k_{\|}>k_1$, which in turn causes the perpendicular component $k_{i\perp}=\sqrt{k_i^2-k_{\|}^2}\equiv i\kappa_{i\perp}$ to be purely imaginary. Physically, these relationships imply that the plasmon modes are nonradiative and are confined near the metal/dielectric interface, with the length scale of transverse confinement determined by $\sim 1/\kappa_{i\perp}$. Furthermore, these plasmon modes cannot couple directly to radiative fields, which have wave vectors $k_{\|}\leqslant k_1$. Of particular interest is the behavior of the plasmon modes in the nanowire limit $|k_i|R\ll 1$. In this limit, all higher-order modes ($|m|\geqslant 1$) exhibit a cutoff as $R\to 0$, as derived in Appendix B, while the $m=0$ fundamental plasmon mode exhibits a unique $k_{\|}\propto 1/R$ behavior. This scaling indicates that the wavelength of these surface plasmons can become strongly reduced relative to the free-space wavelength. Physically, in this limit, the $m=0$ mode can be interpreted approximately as a quasistatic configuration of field and associated charge density wave on the wire. As such, R becomes the only relevant length scale, as the length scales $1/|k_i|$ associated with electrodynamic behavior become unimportant. From the $1/R$ scaling of $k_{\|}$, it also follows that $\kappa_{1\perp}\propto 1/R$. This implies that the field outside the wire becomes tightly localized on a scale $\propto R$ around the metal surface, leading to a small effective transverse mode area that scales like $A_{\text{eff}}\propto R^2$. In particular, it is possible for this mode to be confined well below the diffraction limit. This effect gives rise to a strong interaction strength with nearby emitters, as will be discussed in following sections. We note that this behavior contrasts sharply with that of, e.g, a subwavelength normal dielectric waveguide or optical fiber, which runs into a "confinement problem," where the evanescent tails outside the device become exponentially large as $R\to 0$.[30]

In practice, ϵ_2 is not purely real but has a small imaginary part corresponding to losses in the metal (heating) at optical frequencies. Its effect is to add a small imaginary component to $k_{\|}$, corresponding to dissipation, as the plasmon propagates along the wire. In the inset of Fig. 2, we plot Re $k_{\|}$/Im $k_{\|}$ for the fundamental mode as a function of R. This quantity is proportional to the decay length in units of the plasmon wavelength $\lambda_{\text{pl}}\equiv 2\pi/\text{Re}\,k_{\|}$. As R decreases, it can be seen that this ratio decreases monotonically but approaches a nonzero constant, as will be explicitly shown below. For silver at $\lambda_0=1$ μm, room temperature, and $\epsilon_1=2$, this constant is approximately 140. The fact that this ratio does not approach zero even as $R\to 0$ is important for potential applications, as it implies that the plasmons can still travel several times the wavelength λ_{pl} for devices of any size. We also note that while all numbers and figures presented here are for room temperature, operating at lower temperatures might somewhat reduce the value of Im ϵ_2 due to decreased losses from phonon-assisted absorption.[31]

We now analyze the fundamental mode more carefully. For $m=0$, one sees in Eq. (1) that one of the two terms on the right-hand side must equal zero. It can be shown that setting the first term to zero corresponds to a TE mode, while the other case corresponds to a TM mode (see Appendix A). The TE mode equation does not have any solutions, and thus, the fundamental mode is a TM mode that satisfies the simplified equation[10,32]

$$\frac{k_2^2}{k_{2\perp}}\frac{J_0'(k_{2\perp}R)}{J_0(k_{2\perp}R)}-\frac{k_1^2}{k_{1\perp}}\frac{H_0'(k_{1\perp}R)}{H_0(k_{1\perp}R)}=0. \tag{2}$$

The fields themselves are given by (see Appendix A)

$$\mathbf{E}_1=b_1\left[\frac{ik_{\|}k_{1\perp}}{k_1^2}H_0'(k_{1\perp}\rho)\hat{\rho}+\frac{{k_{1\perp}}^2}{k_1^2}H_0(k_{1\perp}\rho)\hat{z}\right]e^{ik_{\|}z},$$

$$\mathbf{E}_2=b_2\left[\frac{ik_{\|}k_{2\perp}}{k_2^2}J_0'(k_{2\perp}\rho)\hat{\rho}+\frac{{k_{2\perp}}^2}{k_2^2}J_0(k_{2\perp}\rho)\hat{z}\right]e^{ik_{\|}z},$$

$$\mathbf{H}_1=\frac{i}{\omega\mu_0}k_{1\perp}b_1H_0'(k_{1\perp}\rho)e^{ik_{\|}z}\hat{\phi},$$

$$\mathbf{H}_2=\frac{i}{\omega\mu_0}k_{2\perp}b_2J_0'(k_{2\perp}\rho)e^{ik_{\|}z}\hat{\phi}, \tag{3}$$

while the boundary conditions between the two dielectrics require that

$$\frac{b_1}{b_2}=\frac{k_{2\perp}}{k_{1\perp}}\frac{J_0'(k_{2\perp}R)}{H_0'(k_{1\perp}R)}. \tag{4}$$

The $1/R$ dependence of $k_\parallel$, $k_{i\perp}$ in the nanowire limit can be confirmed mathematically by considering the nonretarded limit, $c \to \infty$. In this case, $k_{i\perp} = \sqrt{k_i^2 - k_\parallel^2} \approx ik_\parallel$ and the mode equation (2) reduces to

$$\frac{\epsilon_2}{\epsilon_1} = \frac{K_0'(k_\parallel R) I_0(k_\parallel R)}{K_0(k_\parallel R) I_0'(k_\parallel R)}, \tag{5}$$

where I_m, K_m are modified Bessel functions. The solution to Eq. (5) requires $k_\parallel R = C$ to be constant and proves the aforementioned scaling law for $k_\parallel$. It is also straightforward to see that when ϵ_2 acquires a small imaginary component, the constant C becomes complex as well, and that $\mathrm{Re}\, k_\parallel / \mathrm{Im}\, k_\parallel = \mathrm{Re}\, C / \mathrm{Im}\, C$ takes on some fixed, nonzero value. No closed-form solution exists for the equation above, although when $|k_\parallel R| \ll 1$ (corresponding to large $|\epsilon_2/\epsilon_1|$), the equation asymptotically approaches

$$\frac{\epsilon_2}{\epsilon_1} = \frac{2}{(\gamma - \log 2 + \log C)(C)^2}, \tag{6}$$

where $\gamma \approx 0.577$ is Euler's constant.

Finally, it should be noted that the components of $\mathbf{E}_i$ in Eq. (3) are proportional to $k_\parallel k_{i\perp}$ or $k_{i\perp}^2$, while $\mathbf{H}_i$ is proportional to $k_{i\perp}$. Thus, in the nanowire limit when $k_\parallel, |k_{i\perp}| \propto 1/R$, the magnetic fields are a factor of R smaller than the electric fields, which is consistent with this mode being roughly a quasistatic configuration.

III. SPONTANEOUS EMISSION NEAR A METAL NANOWIRE

The small mode volume associated with the fundamental plasmon mode of a nanowire offers a possible mechanism to achieve strong coupling with nearby optical emitters, in analogy to the methods of Refs. 22–25. In this section, we derive more rigorously the interaction between an emitter and an infinite, cylindrical nanowire, and show that under certain circumstances the small mode volume leads to strongly preferential spontaneous emission into the guided plasmon modes via a mechanism equivalent to the Purcell effect[33] in cavity QED.

The spontaneous emission rate of a dipole emitter, in general, becomes altered from its free-space value in the presence of some dielectric body. In our system of interest, the dipole can possibly lose power radiatively to propagating photon modes through excitation of the guided plasmon modes or through nonradiative loss (heating) in the wire. The dipole in consideration can physically be formed by a single atom, a defect in a solid-state system, or any other system with a dipole-allowed transition. In Sec. III A, we calculate the radiative and nonradiative rates using a quasistatic approach, while waiting until Sec. III B to treat the plasmon decay rate more thoroughly. In Sec. III C, we show how the efficiency of emission into the plasmon modes can be optimized to yield Purcell factors in excess of $\sim 10^3$, and discuss the physical origins of this limit.

A. Radiative and nonradiative decay rates

In this section, we derive formulas for the decay rates of a dipole near a metal nanowire into radiative and nonradiative channels. This calculation closely follows that of Ref. 34, but is briefly presented here for completeness.

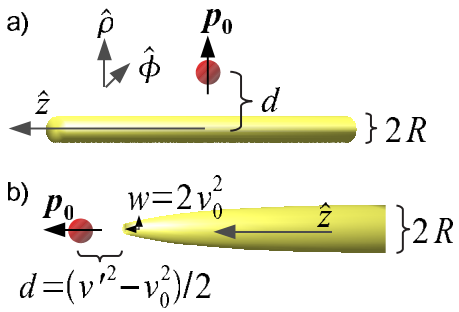

FIG. 3. (Color online) (a) A dipole emitter positioned a distance d from the center of a nanowire. For the calculations presented, the orientation of the dipole moment is assumed to be along $\hat{\rho}$. (b) A dipole emitter positioned near the end of a nanotip. In terms of parabolic coordinates, the physical distance d between the end of the tip and the emitter is given by $d = (v'^2 - v_0^2)/2$, while the curvature parameter $w = 2v_0^2$. For the nanotip, only a dipole oriented parallel to $\hat{z}$ couples to the fundamental plasmon mode.

It is well known that spontaneous emission rates can be obtained via classical calculations of the fields due to an oscillating dipole near the dielectric body,[35] and this method will be employed here. Specifically, we consider an (classical) oscillating dipole $\mathbf{p_0} e^{-i\omega t}$ positioned a distance d from the center of the wire, and wish to calculate the total fields of the system [see Fig. 3(a)]. Before proceeding further, we first note that, in general, the solution will depend on the orientation of the dipole moment in addition to its position. Again taking $\hat{z}$ to be along the axis of the wire, we note that the fundamental surface plasmon mode will not couple to a dipole moment $\mathbf{p_0} \propto \hat{\phi}$ oriented along the azimuthal axis, due to the azimuthal symmetry of this mode. In the following calculations for the nanowire, for concreteness we will consider a dipole oriented along the radial direction ($\mathbf{p_0} \propto \hat{\rho}$) while noting that the calculation for an orientation along $\hat{z}$ yields qualitatively similar results. For nanostructures, one can make a simplification by considering the fields in the quasistatic limit ($\mathbf{H} \approx 0$),[34] which satisfy

$$\nabla \cdot \mathbf{D} = \rho_{\mathrm{ext}}, \tag{7}$$

$$\nabla \times \mathbf{E} = 0. \tag{8}$$

Here, $\rho_{\mathrm{ext}}(\mathbf{r})$ is the external charge density. In taking the quasistatic limit, we essentially assume that we are considering length scales r over which the phases $k_i r$ associated with the electrodynamic Green's function $G_i(\mathbf{r}) \sim e^{ik_i r}/r$ are negligible, so that this function can be approximated by the electrostatic version, $G_i(\mathbf{r}) \sim 1/r$. In the system of interest, the external source is a dipole located at position $\mathbf{r}'$ outside the wire (with radial coordinate $\rho' = d$), so that

$$\rho_{\mathrm{ext}}(\mathbf{r}, \mathbf{r}') = (\mathbf{p_0} \cdot \nabla') \delta(\mathbf{r} - \mathbf{r}'). \tag{9}$$

For simplicity, we omit the harmonic time dependence from our expressions for the source and all fields. Note that the $\delta(\mathbf{r} - \mathbf{r}')$ term above corresponds to a (unitless) point charge source, while the operator $(\mathbf{p_0} \cdot \nabla')$ generally converts the

point charge solution to that of a dipole. It is therefore convenient to write $\mathbf{E}_i$ in a similar form,

$$\mathbf{E}_i(\mathbf{r},\mathbf{r}') = -\nabla(\mathbf{p_0}\cdot\nabla')\Phi_i(\mathbf{r},\mathbf{r}'), \tag{10}$$

where $\Phi_i(\mathbf{r},\mathbf{r}')$ are "pseudopotentials" that satisfy $\nabla^2\Phi_1 = -\delta(\mathbf{r}-\mathbf{r}')/\epsilon_0\epsilon_1$ and $\nabla^2\Phi_2=0$. Here, the indices 1 and 2 again denote the regions outside and inside the cylinder, respectively. Φ physically corresponds to the potential due to a point charge at $\mathbf{r}'$, while the dipole potential follows from $\Phi_{dip}\equiv(\mathbf{p_0}\cdot\nabla')\Phi$.

To solve for the fields, it is convenient to further separate Φ_1 into "free" and "reflected" components Φ_0 and Φ_r, respectively, where Φ_r represents a source-free contribution that ensures that boundary conditions are satisfied, and Φ_0 is the solution for a point charge in a medium of uniform electric permittivity ϵ_1. We will expand the known source term Φ_0 in a basis appropriate for the cylindrical geometry and expand the source-free terms $\Phi_{r,2}$ in a similar basis that satisfies Laplace's equation ($\nabla^2\Phi_{r,2}=0$). The unknown coefficients multiplying the basis functions of $\Phi_{r,2}$ will then be determined by enforcing the proper boundary conditions at the dielectric interface. These expansions are given by

$$\begin{aligned}\Phi_0(\mathbf{r},\mathbf{r}') &= \frac{1}{4\pi\epsilon_0\epsilon_1}\frac{1}{|\mathbf{r}-\mathbf{r}'|}\\ &= \frac{1}{2\pi^2\epsilon_0\epsilon_1}\sum_{m=0}^{\infty}(2-\delta_{m,0})\cos[m(\phi-\phi')]\\ &\quad\times\int_0^{\infty}dh\cos[h(z-z')]K_m(h\rho')I_m(h\rho)\\ &\quad(\rho<\rho'),\end{aligned} \tag{11}$$

$$\begin{aligned}\Phi_r(\mathbf{r},\mathbf{r}') &= \frac{1}{2\pi^2\epsilon_0}\sum_{m=0}^{\infty}(2-\delta_{m,0})\cos[m(\phi-\phi')]\\ &\quad\times\int_0^{\infty}dh\alpha_m(h)\cos[h(z-z')]K_m(h\rho')K_m(h\rho),\end{aligned} \tag{12}$$

$$\begin{aligned}\Phi_2(\mathbf{r},\mathbf{r}') &= \frac{1}{2\pi^2\epsilon_0}\sum_{m=0}^{\infty}(2-\delta_{m,0})\cos[m(\phi-\phi')]\\ &\quad\times\int_0^{\infty}dh\beta_m(h)\cos[h(z-z')]K_m(h\rho')I_m(h\rho),\end{aligned} \tag{13}$$

where $\alpha_m(h)$ and $\beta_m(h)$ thus far are unknown amplitude coefficients. We obtain a set of two coupled equations for $\alpha_m(h)$ and $\beta_m(h)$ by requiring continuity of Φ and $\mathbf{D}_\perp$ at the boundary, $\rho=R$. Because of the translational symmetry of the system, these equations are uncoupled in h and can easily be solved (this is in contrast to the case where translational symmetry is broken due to surface roughness, as discussed in Sec. VI). The solutions are given by[34]

$$\alpha_m(h) = \frac{(\epsilon-1)I_m'(hR)I_m(hR)}{\epsilon_1 I_m(hR)K_m'(hR)-\epsilon_2 K_m(hR)I_m'(hR)},$$

$$\beta_m(h) = \frac{I_m(hR)K_m'(hR)-K_m(hR)I_m'(hR)}{\epsilon_1 I_m(hR)K_m'(hR)-\epsilon_2 K_m(hR)I_m'(hR)}, \tag{14}$$

where we have defined $\epsilon\equiv\epsilon_2/\epsilon_1$. Note that Eq. (14) along with Eqs. (11)–(13) gives the total electric field of the dipole and wire system.

To calculate the radiative emission into free space, we consider the far-field properties of the system. Physically, the presence of the emitter induces some dipole moment $\delta\mathbf{p}$ in the nanowire, which results in a total radiated power proportional to the square of the total dipole moment of the system, $P_{\mathrm{rad}}\propto\Gamma_{\mathrm{rad}}\propto|\mathbf{p_0}+\delta\mathbf{p}|^2$. We can determine $\delta\mathbf{p}$ by finding the dipolelike contribution to the reflected potential $\Phi_{dip,r}=(\mathbf{p_0}\cdot\nabla')\Phi_r(\mathbf{r},\mathbf{r}')$ far away from the source, which on physical grounds must behave like ρ^{-2} for large ρ. It is straightforward to show that the $m=1$ term in Eq. (12) is responsible for this contribution, with all other m terms yielding faster decays in ρ. Because of the asymptotic behavior of $K_m(x)\approx\sqrt{\pi/2x}e^{-x}$ when $x\gg1$, for large ρ the integrand in Eq. (12) is significant only over a small region $h\lesssim\rho^{-1}$. As a result, we can safely replace $K_1(h\rho')$ and $\alpha_1(h)$ by their expansions around $h=0$. After this simplification, the integral can, in fact, be evaluated exactly and yields

$$\Phi_r^{(m=1)}\approx-\frac{1}{4\pi\epsilon_0\epsilon_1}\frac{\epsilon-1}{\epsilon+1}\cos(\phi-\phi')\frac{R^2}{\rho'}\frac{\rho}{[\rho^2+(z-z')^2]^{3/2}}, \tag{15}$$

with a corresponding reflected potential

$$\begin{aligned}\Phi_{dip,r}^{(m=1)}(\mathbf{r},\mathbf{r}') &= (\mathbf{p_0}\cdot\nabla')\Phi_r^{(m=1)}(\mathbf{r},\mathbf{r}')\\ &\approx\frac{p_0}{4\pi\epsilon_0\epsilon_1}\frac{\epsilon-1}{\epsilon+1}\cos(\phi-\phi')\frac{R^2}{d^2}\frac{\rho}{(\rho^2+z^2)^{3/2}},\end{aligned} \tag{16}$$

for the choice of parameters $\rho'=d$, $z'=0$, and $\mathbf{p_0}=p_0\hat{\rho}$. Comparing Eq. (16) to the potential due to a dipole $\delta\mathbf{p}$ in uniform dielectric ϵ_1, $V_{\delta\mathbf{p}}=\frac{\delta\mathbf{p}\cdot\mathbf{r}}{4\pi\epsilon_0\epsilon_1 r^3}$, we can readily identify

$$\delta\mathbf{p} = p_0\frac{\epsilon-1}{\epsilon+1}\frac{R^2}{d^2}\hat{\rho} \tag{17}$$

as the induced dipole moment in the wire, from which it follows that the radiative spontaneous emission rate is given by[34]

$$\frac{\Gamma_{\mathrm{rad}}}{\Gamma_0} = \left|1+\frac{\epsilon-1}{\epsilon+1}\frac{R^2}{d^2}\right|^2 \quad (d\gtrsim R). \tag{18}$$

Here, Γ_0 is defined to be the spontaneous emission rate of the emitter in uniform dielectric ϵ_1.[36] Away from the plasmon resonance ($\epsilon\approx-1$), the radiative decay rate changes slightly from Γ_0 and reflects some moderate change in the radiative density of states in the vicinity of the nanowire.

To calculate the other decay rates, one utilizes the fact that the total power loss of an oscillating dipole is proportional to

the electric field in quadrature at the dipole's location, specifically, $\Gamma_{\text{total}} \propto \text{Im}[\mathbf{p_0}\cdot\mathbf{E}_1(\mathbf{r}',\mathbf{r}')]$. Having divided up $\mathbf{E}_1$ into free and reflected components, the contribution to $\mathbf{E}_1$ from the free field simply is associated with the decay rate in uniform dielectric ϵ_1, and thus, we concentrate on the contribution from $\Phi_r(\mathbf{r},\mathbf{r}')$. First, we note that the coefficient $\alpha_0(h)$ derived in Eq. (14) contains a pole at the point where the denominator vanishes. This pole corresponds to an excitation of a natural mode (the fundamental plasmon mode) of the system. This can immediately be seen by comparing the denominator of α_0 to Eq. (5), which gives the plasmon mode in the nanowire limit. The pole lies at $h=C/R$ and agrees with the plasmon wave vector derived in Sec. II, as expected. Evaluating the contribution of this pole to $\mathbf{E}_r(\mathbf{r}',\mathbf{r}')$ gives the decay rate into the fundamental plasmon mode, and is discussed more carefully in the next section. At the same time, in the limit $d\to R$, one expects some type of divergence to occur in the nonradiative decay rate. Physically, as the emitter approaches the wire edge, the divergence results from the large currents in the wire generated by the near field of the dipole and their resulting dissipation. We can find the leading-order term to this divergent decay rate by carefully evaluating the leading-order divergence in the reflected field.

The mathematical origin of the divergence as $d\to R$ is the significant contribution to Φ_r of an infinite number of terms in m. Specifically, in this limit, for a dipole oriented along $\hat{\rho}$,

$$\begin{aligned}\frac{\Gamma_{\text{non-rad}}}{\Gamma_0} &\approx \frac{6\pi\epsilon_0}{k_0^3\sqrt{\epsilon_1}}\frac{\text{Im}\,\hat{\rho}\cdot\mathbf{E}_r(\mathbf{r}',\mathbf{r}')}{p_0}\\ &= -\frac{6\pi\epsilon_0}{k_0^3\sqrt{\epsilon_1}}\,\text{Im}\,\hat{\rho}\cdot\nabla(\hat{\rho}\cdot\nabla')\Phi_r(\mathbf{r},\mathbf{r}')\big|_{\mathbf{r}=\mathbf{r}'}\\ &\approx -\frac{6}{\pi k_0^3\sqrt{\epsilon_1}}\sum_{m=1}^{\infty}\int_0^{\infty} dh\, h^2 K_m'(hd)^2\,\text{Im}\,\alpha_m(h)\\ &\equiv \frac{6}{\pi k_0^3\sqrt{\epsilon_1}}\sum_{m=1}^{\infty}\int_0^{\infty} dh f_m(h,d,R). \end{aligned} \tag{19}$$

The asymptotic behavior of the functions f_m is given by

$$f_m(h,d,R) \approx \begin{cases} \dfrac{m}{2d^2\epsilon_1}\,\text{Im}\left(\dfrac{\epsilon-1}{\epsilon+1}\right)\left(\dfrac{R}{d}\right)^{2m}, & h\to 0\\ \dfrac{h}{2d\epsilon_1}\,\text{Im}\left(\dfrac{\epsilon-1}{\epsilon+1}\right)e^{-2h(d-R)}, & h\to\infty. \end{cases} \tag{20}$$

From the above expressions, we see that f_m as a function of h has a characteristic width of about $[2(d-R)]^{-1}$, yet, at the same time, the quantity $m(R/d)^{2m}$ reaches a maximum around $\tilde{m}\approx\frac{d}{2(R-d)}$ as $d\to R$. This confirms the nonvanishing contribution of an infinite number of terms in m to the decay rate. The exact behavior of the functions f_m is well modeled by a Lorentzian approximation,

$$f_m(h,d,R) \approx \frac{\dfrac{m}{2d^2\epsilon_1}\,\text{Im}\left(\dfrac{\epsilon-1}{\epsilon+1}\right)\left(\dfrac{R}{d}\right)^{2m}}{1+h^2(d-R)^2}, \tag{21}$$

which allows the integration and sum in Eq. (19) to be performed exactly. The resulting decay rate is given by

$$\frac{\Gamma_{\text{nonrad}}}{\Gamma_0} \approx \frac{3}{16k_0^3(d-R)^3\epsilon_1^{3/2}}\,\text{Im}\left(\frac{\epsilon-1}{\epsilon+1}\right). \tag{22}$$

Note that for $|\epsilon|\gg 1$ and small $\text{Im}\,\epsilon$, $\text{Im}\left(\frac{\epsilon-1}{\epsilon+1}\right) \approx 2\,\text{Im}\,\epsilon/(\text{Re}\,\epsilon)^2$, which makes it clear that the nonradiative spontaneous emission rate is proportional to the dissipative part of the electric permittivity.

B. Decay rate into plasmon modes

In this section, we quantify the spontaneous emission rate Γ_{pl} of a dipole into the surface plasmon modes on a nanowire by evaluating the contribution of the pole in $\alpha_0(h)$ to the field seen by the dipole. Before proceeding further, we first note that in the presence of metal losses, the distinction between Γ_{pl} and Γ_{nonrad} is not perfectly well defined, since the plasmons eventually dissipate due to heating as well. Thus, for concreteness, we will define Γ_{pl} to be the decay rate resulting from the pole in the limit that $\text{Im}\,\epsilon_2=0$, and take the plasmon wave vector $k_{\|}$ and C to be purely real in this section. In particular, for a dipole oriented along $\hat{\rho}$,

$$\begin{aligned}\frac{\Gamma_{\text{pl}}}{\Gamma_0} &= \frac{6\pi\epsilon_0}{k_0^3\sqrt{\epsilon_1}}\left[\frac{\text{Im}\,\hat{\rho}\cdot\mathbf{E}_r(\mathbf{r}',\mathbf{r}')}{p_0}\right]_{pole}\\ &= -\frac{6\pi\epsilon_0}{k_0^3\sqrt{\epsilon_1}}\,\text{Im}[\hat{\rho}\cdot\nabla(\hat{\rho}\cdot\nabla')\Phi_r(\mathbf{r},\mathbf{r}')\big|_{\mathbf{r}=\mathbf{r}'}]_{pole}\\ &= -\frac{3}{\pi k_0^3\sqrt{\epsilon_1}}\,\text{Im}\left[\int_0^{\infty} dh\, h^2 K_1^2(hd)\alpha_0(h)\right]_{pole}, \end{aligned} \tag{23}$$

where we have explicitly indicated that we are interested in the pole contribution to the expressions above. The behavior of $\alpha_0(h)$ around the pole's vicinity is given by

$$\alpha_0(h) \approx \frac{1}{\epsilon_1}\frac{(\epsilon_2-\epsilon_1)I_1(C)I_0(C)}{(h-C/R)R\dfrac{d\chi(C)}{dx}}, \tag{24}$$

where

$$\chi(x) = \epsilon_1 I_0(x)K_0'(x) - \epsilon_2 K_0(x)I_0'(x). \tag{25}$$

Substituting this into Eq. (23) then yields the decay rate

$$\Gamma_{\text{pl}} = \alpha_{\text{pl}}\Gamma_0\frac{K_1^2(Cd/R)}{(k_0R)^3} \approx \alpha_{\text{pl}}\Gamma_0\frac{K_1^2(\kappa_{1\perp}d)}{(k_0R)^3}, \tag{26}$$

where we have identified $\kappa_{1\perp}\approx C/R$ in the nanowire limit. The coefficient α_{pl} is given by

$$\alpha_{\text{pl}} = \frac{3(\epsilon_1-\epsilon_2)}{\epsilon_1^{3/2}}\frac{C^2I_1(C)I_0(C)}{d\chi(C)/dx} \tag{27}$$

and most importantly depends only on $\epsilon_{1,2}$.

The $\sim(1/R)^3$ scaling of the spontaneous emission rate into plasmons indicates that this process can be strongly enhanced by using a small wire. One can gain some physical understanding of the result and its relation to the Purcell effect in cavity QED by considering the quantum mechanical derivation of the spontaneous emission rate via Fermi's golden rule. This rule states that, once the plasmon modes are quantized, the decay rate is given by

$$\Gamma_{\mathrm{pl}} = 2\pi g^2(\mathbf{r},\omega) D(\omega), \tag{28}$$

where $g(\mathbf{r},\omega)$ is the position-dependent, dipole-field interaction matrix element, and $D(\omega)$ is the plasmon density of states on the nanowire. Here, $g(\mathbf{r},\omega)=\vec{\wp}\cdot\vec{\mathcal{E}}(\mathbf{r})/\hbar$ itself depends on the dipole matrix element $\vec{\wp}=\langle e|e\mathbf{r}|g\rangle$ of the emitter, where $|g\rangle$ ($|e\rangle$) is the ground (excited) state involved in the transition, and on the electric field per photon $\vec{\mathcal{E}}(\mathbf{r})$ for the surface plasmon modes. On dimensional grounds, the electric field per photon can be written in the form $\vec{\mathcal{E}}(\mathbf{r}) = \sqrt{\hbar\omega/\epsilon_0 V_{\mathrm{eff}}}[\mathbf{E}(\mathbf{r})/E_{max}]$, where V_{eff} is an effective mode volume characterizing the confinement of each mode, $\mathbf{E}(\mathbf{r})$ is the classical field profile for the surface plasmon modes given in Eq. (3), and $E_{max}=\max|\mathbf{E}(\mathbf{r})|$. The mode volume can be estimated by normalizing the field energy to one quantum (again, ignoring Im ϵ_2),

$$\hbar\omega \sim L\int d^2\boldsymbol{\rho}\epsilon_0 \frac{d}{d\omega}[\omega\epsilon(\boldsymbol{\rho},\omega)]|\vec{\mathcal{E}}(\boldsymbol{\rho})|^2. \tag{29}$$

Here, the two-dimensional integral is performed over the directions transverse to the wire axis, and L is the quantization length, set by the wire length, which is assumed to be much longer than all other relevant length scales. In the end, L will disappear from the physical quantities of interest (e.g., the spontaneous emission rate). The integrand appearing in Eq. (29) gives the correct expression for the classical electric energy density for a field in a dispersive medium.[27] Because the fields are primarily electric in the nanowire limit, we have safely ignored the magnetic field contribution to the energy density. Performing this normalization for the fundamental plasmon modes, one finds that $V_{\mathrm{eff}}\propto R^2 L$, which physically implies that these modes are transversely confined to an area on the order of the wire size. The constant of proportionality depends only on the electric permittivities of the system. For a dipole oriented along $\hat{\rho}$, one then finds that $g^2(\mathbf{r})\propto K_1^2(\kappa_{1\perp}d)/(R^2L)$, which shows that the strong field-emitter coupling directly arises from the tight field confinement. At the same time, the density of states for the plasmon modes is given by $D(\omega)\sim(L/2\pi)(dk_{\parallel}/d\omega)$, and is inversely proportional to the group velocity. The group velocity for plasmons is strongly reduced due to the large plasmon wave vector $k_{\parallel}\propto 1/R$ on a nanowire, and consequently, this gives rise to $a\sim 1/R$ enhancement in the density of states. Combining all of these results into Eq. (28) yields

$$\Gamma_{\mathrm{pl}} \propto \Gamma_0 \frac{K_1^2(\kappa_{1\perp}d)^2}{(k_0R)^3}, \tag{30}$$

where again the constant of proportionality depends only on the electric permittivities. We emphasize that in the quantum mechanical interpretation, one achieves a factor of $\sim 1/R$ enhancement in the spontaneous emission rate due to a reduction in the plasmon group velocity and a $\sim 1/R^2$ enhancement due to the small effective mode area.

C. Purcell factor of a nanowire

Comparing the spontaneous emission rates given by Eqs. (18), (22), and (26), we now qualitatively discuss the behavior one should expect as the position of the emitter is varied. In the limit that $d/R \gg 1$, the emitter feels no effect from the wire and the total spontaneous emission rate is close to the radiative rate Γ_0 in a uniform dielectric medium. As one brings the emitter closer to the wire surface, the change in the electromagnetic mode structure near the wire results in some modified radiative decay rate Γ_{rad} which never exceeds approximately $4\Gamma_0$ for large $|\epsilon|$. When the emitter position d approaches $d\sim 1/\kappa_{1\perp}\sim R/|C|$, the emitter starts to interact with the localized plasmon fields, with a corresponding rate of emission into plasmons scaling with wire size like $1/R^3$. The emission rate into plasmons continues to grow as the emitter is brought even closer to the wire edge, $d\to R$. However, the efficiency or probability of plasmon excitation eventually decreases due to the large nonradiative decay rate experienced by the dipole very near the wire, which diverges like $1/(d-R)^3$. We thus expect some optimal efficiency of spontaneous emission into the plasmon modes to occur when the emitter is positioned at a distance $\mathcal{O}(R)$ away from the wire edge, and for this optimal efficiency to improve as $R\to 0$.

The efficiency of coupling to the plasmon modes can be characterized by a "Purcell factor" that is defined by the ratio $P=\Gamma_{\mathrm{pl}}/\Gamma'$, where $\Gamma'=\Gamma_{\mathrm{rad}}+\Gamma_{\mathrm{nonrad}}$ denotes the total emission rate into channels other than the fundamental plasmon mode. Generally, P depends on both the wire size and the position d of the emitter. In Fig. 4(a), we have numerically evaluated the spontaneous emission rates and plotted the Purcell factor as a function of wire radius R, optimized over the emitter position. As $R\to 0$, the optimized Purcell factor P exceeds $\sim 10^3$, indicating that the probability of emission into the plasmons approaches almost unity.[37] Examining this limit more carefully, it can be shown that the "error rate," in fact, approaches a small quantity $\Gamma'/\Gamma_{\mathrm{total}}\propto \mathrm{Im}\,\epsilon/(\mathrm{Re}\,\epsilon)^2$, which explicitly indicates that this process is ultimately limited by material losses. Again, we emphasize that these properties are specifically a result of the conducting properties of the nanowire. This can be contrasted with emission into the guided modes of a subwavelength optical fiber, which drops exponentially as $R\to 0$ due to the weak confinement of these guided modes.[34]

Finally, we note that while the decay rates obtained in the quasistatic approximation provide a simple understanding of the system, the quantitative predictions may begin to break down even for moderate-sized wires (when $|k_i|R\gtrsim 1$). Physically, the effective mode area A_{eff} and group velocity $d\omega/dk_{\parallel}$ start to scale more slowly than $\sim R^2$ and $\sim R$, respectively, for moderate-sized wires. The quasistatic approximation can then significantly underestimate the decay rate into plasmons, Γ_{pl}, and the corresponding Purcell factors. This may

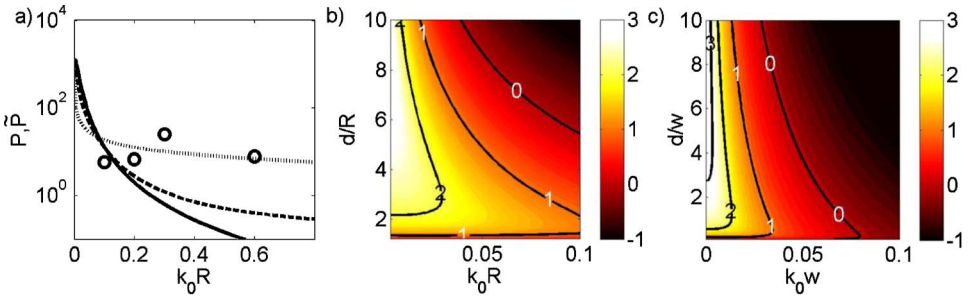

FIG. 4. (Color online) (a) Solid line: Maximum Purcell factor $P=\Gamma_{\mathrm{pl}}/\Gamma'$ for a nanowire, plotted as a function of R and optimized over the emitter position. Here, P is calculated in the quasistatic approximation. Dashed line: Same quantity, obtained by exact electrodynamic calculations. Dotted line: Effective Purcell factor $\tilde{P}(R)=\tilde{\Gamma}_{\mathrm{pl}}(R)/\tilde{\Gamma}(R)$ for a nanotip of final radius R, optimized over nanotip shape and emitter position. Solid points: Same quantity, calculated using numerical simulations (boundary element method). (b) Contour plot of $\log_{10} P$ for a nanowire, as functions of R and d/R. (c) Contour plot of $\log_{10} P$ for a nanotip, as functions of w and d/w.

be important experimentally, for example, since it implies that one need not resort to very small wires to achieve moderate Purcell factors. Thus, using the electrodynamic Green's function methods of Refs. 34 and 38, we have also obtained exact electrodynamic solutions of the fields created by an oscillating dipole near a cylinder, and used these solutions to find the corresponding decay rates. In Fig. 4(a), we have plotted the numerically optimized Purcell factors using these exact electrodynamic results. It can be seen that the quasistatic and exact results agree well in the nanowire limit, but for larger wires, the exact results predict significantly larger values of P. In Fig. 4(b), we plot the Purcell factor as functions of both wire size and emitter position (using the exact results). Here, it can be seen that achieving a large Purcell factor does not depend too sensitively on the placement of the emitter, which indicates that the strong coupling is a robust effect.

IV. SPONTANEOUS EMISSION NEAR A NANOTIP

In Secs. II and III, we derived and discussed the physics of plasmon modes on a nanowire and the spontaneous emission of a nearby dipole emitter. It was seen that the tight transverse confinement of the plasmon modes leads to a large Purcell factor for an optimally positioned dipole emitter as the wire size decreases. At the same time, however, it is evident that the tighter confinement is accompanied by enhanced losses as the plasmon propagates, and also by a large reduction in the plasmon wavelength λ_{pl} that could make outcoupling more difficult. Such factors could clearly impose limits for applications such as quantum information, but can be circumvented with simple design improvements. In this section, we investigate one specific design, a metallic nanotip [see Fig. 3(b)]. As in the nanowire case, one expects a subwavelength plasmon mode volume, determined in this case by the tip curvature, and an associated enhancement of emission into the plasmon modes. Here, however, one expects propagative losses to be less severe, because the plasmons will become less tightly confined as they propagate along the tip and as the tip expands. This expansion also results in a gradual increase in the plasmon wavelength along the nanotip. For the nanotip, we are not able to obtain full electrodynamic solutions for the plasmon modes. However, in a manner similar to that described in Sec. III, we will calculate all of the relevant decay rates in the quasistatic limit and describe an approximate method to calculate the propagative losses along the nanotip. We will also compare these results to those obtained via fully electrodynamic numerical simulations, and we find that these two approaches agree closely.

In the following, we will consider a nanotip whose surface can be parametrized as a paraboloid of revolution with symmetry along the z axis [see Fig. 3(b)]. Specifically, we suppose that the surface of the nanotip is described by

$$z=\frac{1}{2}\left(\frac{x^2+y^2}{v_0^2}-v_0^2\right), \tag{31}$$

a paraboloid of revolution with apex at $z=-v_0^2/2$ (the reason for the offset of the apex will become apparent below). We now introduce a transformation to parabolic coordinates,

$$x=uv\cos\phi, \tag{32}$$

$$y=uv\sin\phi, \tag{33}$$

$$z=\frac{1}{2}(u^2-v^2). \tag{34}$$

While these coordinates may seem awkward (note, for example, that u and v have units of $\sqrt{\text{length}}$), they are convenient for deriving expressions for the fields and spontaneous emission rates, which we will then express in more "natural" coordinates at the end of the calculation. In parabolic coordinates, the nanotip profile of Eq. (31) is defined by a surface of constant $v=v_0$. More generally, any constant v defines some paraboloid of revolution in this system, while the unit vectors $\hat{u}$ and $\hat{v}$ run normally and tangentially to these surfaces, respectively.

Now, as in the nanowire case, we are interested in finding the quasistatic field solution for a point charge source in the vicinity of the nanotip, from which we can obtain the field due to a dipole $\mathbf{p_0}$. In particular, we seek solutions of the total field of the form Eq. (10) with appropriate boundary conditions. Like before, we separate the pseudopotential Φ_1

outside the nanotip into its free and reflected components $\Phi_{0,r}$, and use an integral representation of the free pseudopotential suitable for parabolic coordinates,

$$\Phi_0(\mathbf{r},\mathbf{r}') = \frac{1}{2\pi\epsilon_0\epsilon_1}\sum_{m=0}^{\infty}(2-\delta_{m,0})\cos m(\phi-\phi')\int_0^{\infty} dq \times qJ_m(qu)J_m(qu')I_m(qv)K_m(qv') \quad (v<v'). \tag{35}$$

Here, the primed coordinates denote the position of the dipole. Because Φ_0 fully accounts for the point source, $\Phi_{r,2}$ then satisfy Laplace's equation. Using separation of variables, it is straightforward to show that the solutions to Laplace's equation are given in parabolic coordinates by $\sim J_m(qu)G_{i,m}(qv)e^{im\phi}$, where $G_{1,m}(qv)=K_m(qv)$ and $G_{2,m}(qv)=I_m(qv)$ are nondivergent functions in their regions of applicability. We then define the following expansions:

$$\Phi_r(\mathbf{r},\mathbf{r}') = \frac{1}{2\pi\epsilon_0\epsilon_1}\sum_{m=0}^{\infty}(2-\delta_{m,0})\cos m(\phi-\phi')\int_0^{\infty} dq \times q\alpha_m(q)J_m(qu')K_m(qv')J_m(qu)K_m(qv), \tag{36}$$

$$\Phi_2(\mathbf{r},\mathbf{r}') = \frac{1}{2\pi\epsilon_0\epsilon_1}\sum_{m=0}^{\infty}(2-\delta_{m,0})\cos m(\phi-\phi')\int_0^{\infty} dq \times q\beta_m(q)J_m(qu')K_m(qv')J_m(qu)I_m(qv), \tag{37}$$

where the coefficients α and β are determined by imposing boundary conditions at the nanotip surface $v=v_0$. Enforcing the continuity of Φ and $\mathbf{D}_\perp$ yields

$$\alpha_m(q) = \frac{(\epsilon_1-\epsilon_2)I_m'(qv_0)I_m(qv_0)}{\epsilon_2 I_m'(qv_0)K_m(qv_0)-\epsilon_1 I_m(qv_0)K_m'(qv_0)}, \tag{38}$$

$$\beta_m(q) = \frac{-\epsilon_1[I_m(qv_0)K_m'(qv_0)-I_m'(qv_0)K_m(qv_0)]}{\epsilon_2 I_m'(qv_0)K_m(qv_0)-\epsilon_1 I_m(qv_0)K_m'(qv_0)}. \tag{39}$$

Note that the coefficients $\alpha_m(q)$, along with Eq. (36), completely determine the reflected field.

The calculation of the radiative and nonradiative spontaneous emission rates proceeds in the same manner as the nanowire case. To calculate Γ_{rad}, we again look for a dipole term in the far field (large v) that corresponds to an induced dipole moment $\delta\mathbf{p}$ in the nanotip, and then use the relationship $\Gamma_{\text{rad}} \propto |\mathbf{p_0}+\delta\mathbf{p}|^2$. At the same time, we look for a divergent contribution to the reflected field at the dipole location as its position v' approaches v_0, which yields the leading term of the nonradiative decay rate through $\Gamma_{\text{nonrad}} \propto \text{Im}[\mathbf{p_0}\cdot\mathbf{E}_r(\mathbf{r}',\mathbf{r}')]$. For concreteness, we will consider a dipole that is located along the z axis [$u'=0$, also see Fig. 3(b)], which yields

$$\mathbf{p_0}\cdot\mathbf{E}_r(\mathbf{r}',\mathbf{r}') = -\frac{p_0^2}{4\pi\epsilon_0\epsilon_1}\int_0^{\infty} dq\frac{q^3}{v'^2}\alpha_1(q)K_1^2(qv') \quad (\mathbf{p_0}\perp\hat{z}),$$

$$\mathbf{p_0}\cdot\mathbf{E}_r(\mathbf{r}',\mathbf{r}') = -\frac{p_0^2}{2\pi\epsilon_0\epsilon_1}\int_0^{\infty} dq\frac{q^3}{v'^2}\alpha_0(q)K_1^2(qv') \quad (\mathbf{p_0}\parallel\hat{z}), \tag{40}$$

as shown in Appendix C. Because of the similarity of the decay rate calculations with those in Sec. III, we simply state the results here, while providing more details in Appendix C. For a dipole positioned along the z axis at $v=v'$, the radiative and nonradiative spontaneous emission rates are given by

$$\frac{\Gamma_{\text{rad}}}{\Gamma_0} = \left|1-\frac{v_0^2}{v'^2}\left(1-\frac{\epsilon_2}{\epsilon_1}\right)\right|^2 \quad (\mathbf{p_0}\parallel\hat{z}),$$

$$\frac{\Gamma_{\text{rad}}}{\Gamma_0} = \left|1+\frac{\epsilon_1-\epsilon_2}{\epsilon_1+\epsilon_2}\frac{v_0^2}{v'^2}\right|^2 \quad (\mathbf{p_0}\perp\hat{z}), \tag{41}$$

and

$$\frac{\Gamma_{\text{nonrad}}}{\Gamma_0} \approx \frac{3}{16k_0^3\epsilon_1^{3/2}}\frac{1}{v'^3(v'-v_0)^3}\text{Im}\left(\frac{\epsilon_2-\epsilon_1}{\epsilon_2+\epsilon_1}\right) \quad (\mathbf{p_0}\perp\hat{z}),$$

$$\frac{\Gamma_{\text{nonrad}}}{\Gamma_0} \approx \frac{3}{8k_0^3\epsilon_1^{3/2}}\frac{1}{v'^3(v'-v_0)^3}\text{Im}\left(\frac{\epsilon_2-\epsilon_1}{\epsilon_2+\epsilon_1}\right) \quad (\mathbf{p_0}\parallel\hat{z}). \tag{42}$$

Finally, we consider the decay rate into the fundamental plasmon mode of the nanotip, which is associated with the contribution of the poles in the integrand of Eq. (40) to $\text{Im}[\mathbf{p_0}\cdot\mathbf{E}_r(\mathbf{r}',\mathbf{r}')]$. Examining the solutions to $\alpha_{0,1}$ given in Eq. (38), one finds that α_1 has no pole in the range $0\leqslant q\leqslant\infty$. Physically, the absence of a pole means that a dipole simultaneously oriented perpendicular to $\hat{z}$ and located along the z axis does not excite the fundamental plasmon mode of the nanotip. This is easily understood since a dipole oriented this way is antisymmetric with respect to 180° rotations about $\hat{z}$, while the plasmon mode is symmetric. On the other hand, α_0 does have a pole corresponding to plasmon excitation. This pole is located at $q_0=C/v_0$, where C is the solution to Eq. (5). q_0 can be considered to be the "wave vector" of the fundamental mode (albeit in parabolic coordinates). Evaluating the contribution of this pole to the field is straightforward and yields a plasmon decay rate

$$\frac{\Gamma_{\text{pl}}}{\Gamma_0} = \frac{3\pi}{k_0^3\epsilon_1^{3/2}}\frac{C^3}{v_0^4v'^2}K_1^2(q_0v')\frac{(\epsilon_1-\epsilon_2)I_1(C)I_0(C)}{d\chi(C)/dx} \quad (\mathbf{p_0}\parallel\hat{z}), \tag{43}$$

$$\frac{\Gamma_{\text{pl}}}{\Gamma_0} = 0 \quad (\mathbf{p_0}\perp\hat{z}), \tag{44}$$

where $\chi(x)$ is defined in Eq. (25). As in the nanowire case, the decay rate Γ_{pl} into the plasmon mode given by Eq. (43) is evaluated in the limit that $\text{Im}\,\epsilon_2=0$, such that q_0 and C are purely real.

Having derived the decay rates in parabolic coordinates, we now define a more natural set of parameters to describe the system [see Fig. 3(b)]. Let us introduce a length scale w that characterizes the curvature of the nanotip via $\rho(z)$

$=\sqrt{wz}$ $(z \geqslant 0)$, where ρ is the radius of the nanotip at position z (note also the corresponding shift in the apex of the tip from $z=-v_0^2/2$ to $z=0$). Furthermore, let $z=-d<0$ be the position of the emitter $[d=(v'^2-v_0^2)/2$ is the distance between the emitter and end of the nanotip]. In terms of these parameters, the spontaneous emission rates derived above for a dipole $\mathbf{p_0} \propto \hat{z}$ positioned along the z axis can be rewritten as

$$\frac{\Gamma_{\mathrm{rad}}}{\Gamma_0} = \left| 1 + \left[1 + (4d/w)\right]^{-1} \left(\frac{\epsilon_2}{\epsilon_1} - 1 \right) \right|^2, \tag{45}$$

$$\frac{\Gamma_{\mathrm{nonrad}}}{\Gamma_0} = \frac{3}{8\epsilon_1^{3/2}} \frac{1}{(k_0 d)^3} \mathrm{Im}\left(\frac{\epsilon_2 - \epsilon_1}{\epsilon_2 + \epsilon_1} \right), \tag{46}$$

$$\frac{\Gamma_{\mathrm{pl}}}{\Gamma_0} = \tilde{\alpha}_{\mathrm{pl}} \frac{1}{(k_0 w)^3 [1 + (4d/w)]} K_1^2 \left[C\sqrt{1 + (4d/w)} \right], \tag{47}$$

where $\tilde{\alpha}_{\mathrm{pl}}$ only depends on $\epsilon_{1,2}$ and is given by

$$\tilde{\alpha}_{\mathrm{pl}} = \frac{24\pi}{\epsilon_1^{3/2}} C^3 \frac{(\epsilon_1 - \epsilon_2) I_1(C) I_0(C)}{d\chi(C)/dx}. \tag{48}$$

As in the nanowire case, one can define a Purcell factor $P=\Gamma_{\mathrm{pl}}/\Gamma'$ for the nanotip, which depends on the curvature parameter w and emitter position d. Optimization of the Purcell factor over the emitter position yields a large enhancement of $P \approx 2.5 \times 10^3$ as $w \to 0$, which is limited ultimately by dissipation in the metal. In Fig. 4(c), we plot P as functions of w and d. Once again, it can be seen that achieving large Purcell factors does not depend too sensitively on the emitter position.

To compare the benefits of the nanotip over the nanowire, the relevant quantity is not just the Purcell factor but how efficiently the generated plasmons can propagate from the end to some larger radius R further down the tip [see Fig. 3(b)]. Because the plasmon modes here were obtained through a quasistatic approximation, this calculation yields no information about dissipative losses as the plasmon propagates along the nanotip. For example, in this limit $\mathbf{H} \approx 0$, so one cannot obtain the Poynting vector for the system. To estimate the effect of propagative losses, however, we can make an eikonal approximation,[39] assuming that the plasmons are emitted completely into the end of the tip $(z=0)$ and that the propagative losses thereafter at any position z are identical locally to those of a nanowire of radius $\rho(z)$. Specifically, the fraction of the total plasmon emission that successfully propagates from the end to some larger radius R is estimated to be

$$\frac{\tilde{\Gamma}_{\mathrm{pl}}(R)}{\Gamma_{\mathrm{pl}}} = \exp\left(-2 \int_0^{z(R)} \mathrm{Im}\, k_{\parallel}[\rho(z)] dz \right). \tag{49}$$

Whereas Γ_{pl} is the spontaneous emission rate into the plasmons, $\tilde{\Gamma}_{\mathrm{pl}}(R)$ is the rate that these emitted plasmons successfully propagate to radius R. It is also convenient to define an effective decay into other channels, $\tilde{\Gamma}'(R)=\Gamma'+[\Gamma_{\mathrm{pl}} - \tilde{\Gamma}_{\mathrm{pl}}(R)]$, which includes the rate at which emitted plasmons are dissipated before reaching R. Similarly, we define an effective Purcell factor for the nanotip, given by $\tilde{P}(R) = \tilde{\Gamma}_{\mathrm{pl}}(R)/\tilde{\Gamma}'(R)$, which characterizes the efficiency that plasmons are generated and propagate successfully to R. In general, this quantity depends both on the emitter position and the curvature of the nanotip. In Fig. 4(a), we plot $\tilde{P}(R)$ when optimized over w and d. It can be seen that the effective Purcell factor for the nanotip compares favorably to the Purcell factor of a nanowire when $k_0 R \gtrsim 0.05$. In other words, the nanotip makes it possible to use these larger sizes to reduce dissipation, without as steep a trade-off in the efficiency of coupling to the plasmons. We note that the nanotip system also has the added benefit of generating guided plasmons along a single direction of propagation away from the end of the tip.

We now discuss the limits of validity of the equations derived above for the nanotip. First, as discussed in Sec. III A, the quasistatic calculation of the decay rates is valid only when one is considering length scales where the electrodynamic Green's function can be approximated by its electrostatic equivalent. For the nanotip, this restricts the regimes of validity to $|k_i|w$, $|k_i|d \ll 1$. An additional set of assumptions is made in using the eikonal approximation to arrive at Eq. (49). Specifically, we have assumed that the change in the radius $\rho(z)$ of the nanotip occurs slowly enough that the wave vector $k_{\parallel}(\rho)$ of the surface plasmon modes can adiabatically follow the nanowire solution at each position z. The adiabaticity condition can be quantified by a parameter $\beta=d[1/\mathrm{Re}\, k_{\parallel}(\rho)]/dz$, which must remain small at all positions z. Assuming, for example, that we are considering sufficiently small length scales that the wave vector $k_{\parallel}[\rho(z)] \approx C/\rho(z)$ follows quasistatic behavior, the condition $\beta \ll 1$ is satisfied only in the region $z \gg z_c$, where $z_c \equiv w/|C^2|$ represents some crossover point between adiabatic and nonadiabatic propagations. Thus, at first glance, the accumulated losses predicted by Eq. (49) in propagating from the end of the tip $(z=0)$ to $z \sim z_c$ appear invalid. We now argue, however, that as long as the upper limit of integration $z(R)$ satisfies $z(R) \gg z_c$, Eq. (49) remains a good approximation for finding the total losses. In particular, we argue that the actual losses from $z=0$ to $z \sim z_c$ are quite small, compared to the losses accumulated in going from $z \sim z_c$ to $z \gg z_c$. In the latter region, the integrand of Eq. (49) is a good approximation, as previously discussed. Then, in the region from $z=0$ to $z \sim z_c$, the specific form of the integrand does not matter, as long as it provides a small overall contribution to the total losses. First, it is straightforward to show that the predicted loss in this region, while incorrect, is small for realistic systems, $\tilde{\Gamma}_{\mathrm{pl}}[R(z_c)]/\Gamma_{\mathrm{pl}} \sim \exp(-\mathrm{Im}\ C/|C|)$. Next, we argue that the actual losses in this region should be small. Physically, the quantity $|q_0|^{-2}=v_0^2/|C|^2 \sim z_c$ determines the fundamental length scale for the nanotip plasmons, since q_0 is the wave vector for the plasmons in parabolic coordinates. Because dissipation can be treated as a small perturbation for realistic systems, the losses should be significant only on length scales much larger than this, just as losses are only relevant on scales much longer than the inverse plasmon wave vector, $1/|k_{\parallel}|$, for the nanowire.

To check the analytical results derived above for the nanotip, we have also performed detailed numerical simulations

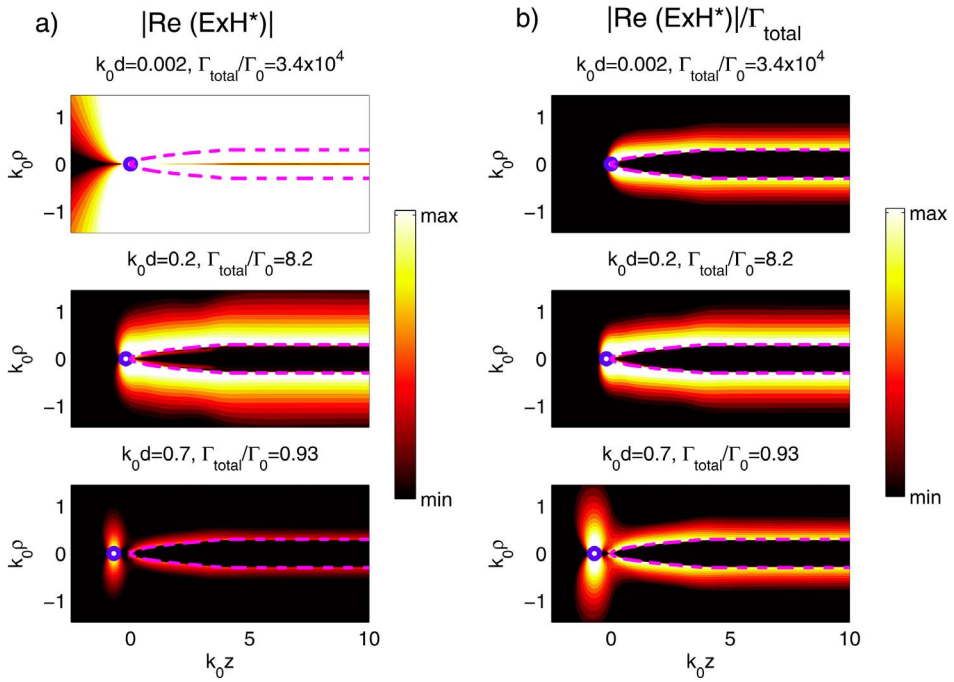

FIG. 5. (Color online) Numerically calculated fields due to a dipole emitter near a conducting nanotip, obtained by the boundary element method. (a) The energy flux $|\mathrm{Re}(\mathbf{E}\times\mathbf{H}^*)|$, in arbitrary units. The position of the emitter is denoted by the blue circles, while the boundary of the nanotip is given by the dotted lines. The plots shown are for a final nanotip radius of $k_0R=0.3$, curvature parameter $k_0w=0.022$, and emitter positions $k_0d=0.002$, 0.2, and 0.7. It can be seen that both the total spontaneous emission rate Γ_{total} and the emission rate into plasmons increase as the emitter is brought closer to the nanotip. (b) The quantity $|\mathrm{Re}(\mathbf{E}\times\mathbf{H}^*)|/\Gamma_{\mathrm{total}}$, for the same parameters. This quantity is proportional to the energy flux normalized by the total power output of the emitter. The $k_0d=0.002$ plot is mostly dark, indicating that most of the decay is into nonradiative channels. The $k_0d=0.2$ case is characterized by bright spots along the entire edge of the nanotip, which indicates efficient plasmon excitation. The $k_0d=0.7$ case exhibits the typical lobe pattern associated with radiative decay of a dipole.

using the boundary element method (BEM).[40] Details of our implementation are given in Appendix D. BEM simulations are fully electrodynamic solvers of Maxwell's equations, and they were used to obtain the classical electromagnetic field solutions of an oscillating dipole emitter $\mathbf{p_0}e^{-i\omega t}$ near a nanotip. The results of a few sample simulations are shown in Fig. 5, for a tip curvature parameter $k_0w=0.022$, final radius $k_0R=0.3$, and varying emitter positions $k_0d=0.002$, 0.2, and 0.7. In Fig. 5(a), we plot the quantity $|\mathrm{Re}(\mathbf{E}\times\mathbf{H}^*)|$, which is proportional to the Poynting vector and corresponds to the total energy flux of the system. The nanotip is assumed to be composed of silver in a surrounding dielectric $\epsilon_1=2$, and its boundary is given by the dotted line, while the emitter positions are denoted by circles. The total spontaneous emission rate is given via $\Gamma_{\mathrm{total}}=(\Gamma_{\mathrm{pl}}+\Gamma')\propto\mathrm{Im}[\mathbf{p_0}\cdot\mathbf{E}_1(\mathbf{r}',\mathbf{r}')]$ and is determined numerically for each configuration by finding the total field at the dipole location. On the other hand, the effective emission rate $\tilde{\Gamma}_{\mathrm{pl}}(R)$ into the plasmons is determined by a best fit of the fields in the region of constant R to the known plasmon solution on a nanowire given in Eq. (3), and then by calculating the total power transport of this best-fit mode through the integrated Poynting vector. This total power is directly proportional to $\tilde{\Gamma}_{\mathrm{pl}}(R)$. The figure confirms the qualitative behavior that we expect and have described previously. In particular, the generated plasmon field and total spontaneous emission rate are largest for very small separations and decrease as the emitter is placed further away from the end of the nanotip. In Fig. 5(b), we plot $|\mathrm{Re}(\mathbf{E}\times\mathbf{H}^*)|/\Gamma_{\mathrm{total}}$, which is proportional to the energy flux normalized by the total power output of the emitter. This quantity yields information about the efficiency of decay into the various channels. For small separations ($k_0d=0.002$), the plot is mostly dark, which indicates that the decay of the dipole is predominantly nonradiative. For $k_0d=0.2$, the maximum (corresponding to bright spots in the plot) is located along the entire surface of the nanotip, which indicates highly efficient plasmon excitation. Here, although the total emission rate into plasmons decreases from the $k_0d=0.002$ case [as seen in Fig. 5(a)], the efficiency increases dramatically due to less competition from nonradiative decay. Finally, for $k_0d=0.7$, the maximum appears as the typical lobe pattern associated with radiative decay.

In Fig. 4(a), we have plotted the numerically optimized values of $\tilde{P}(R)$ for a few values of R. It can be seen that the values obtained through analytical approximations and numerical BEM closely agree. Unlike the theoretical predictions, however, the numerically calculated error probability does not increase monotonically with R. We believe that the origin of this is that, for the numerically optimized parameters, the condition $R\gg\rho(z_c)$ under which the theoretical predictions hold is only weakly satisfied, and the excitation region for the plasmons cannot strictly be thought of as a single point at the end of the tip ($z=0$).

V. SINGLE-PHOTON GENERATION VIA COUPLING TO DIELECTRIC WAVEGUIDE

We have shown in previous sections that a single emitter can spontaneously emit into the guided plasmon modes of a nearby nanostructure with high probability. This prospect of efficient conversion between an excitation of the emitter and a single photon has a number of applications in the fields of quantum computing and quantum information. In this section, we consider one particular application involving the use of such a system as an efficient single-photon source. The concepts behind single-photon generation on demand with an individual emitter in a cavity have been discussed elsewhere[41–43] and will not be presented in detail here. We note also that the ideas behind single-photon sources can be extended to create long-distance entanglement between emitters, as detailed, e.g, in Ref. 44.

Because of dissipative losses in metals, the plasmon modes are not directly suitable as carriers of information over long distances. We show, however, that plasmonic devices can serve as an effective intermediate step, and in particular, can be efficiently outcoupled to the modes of a copropagating dielectric waveguide. The single-photon device is illustrated schematically in Fig. 1. In Fig. 1(a), an optically addressable emitter with multiple internal levels sits in the vicinity of a conducting nanowire. The emitter is strongly coupled to the nanowire, such that single photons on demand can be generated with high efficiency in the plasmon modes by external manipulation of the emitter. The addressability of the emitter along with the internal levels allows for shaping of this single-photon pulse,[45] as illustrated in Fig. 1(b). Here, a three-level emitter is shown with two ground or metastable states $|s\rangle$ and $|g\rangle$. We assume that the transition between $|s\rangle$ and excited state $|e\rangle$ is decoupled from the plasmon modes, due to, e.g, the orientation of its dipole moment, but that the states are coupled via some classical control field with Rabi frequency $\Omega(t)$. We also assume that the transition $|e\rangle$-$|g\rangle$ is coupled via the plasmon modes of the nanowire; i.e., the state $|e\rangle$ can decay at a rate Γ_{pl} into $|g\rangle$ by emitting a photon into the plasmon modes. In addition, there is a small rate Γ' at which the excited state can decay without emitting a plasmon. A single photon in the plasmon modes of the nanowire is generated with high probability by initializing the emitter in $|s\rangle$ and exciting the transition $|s\rangle$-$|e\rangle$ with the control field $\Omega(t)$. The decay of $|e\rangle$ into $|g\rangle$ and the generation of an outgoing single plasmon then occur with high probability, with the shape of the single-photon wave packet determined by the shape of $\Omega(t)$. We further assume that the plasmon is then evanescently coupled to the nearby dielectric waveguide [see Fig. 1(a)], which copropagates with the nanowire over some distance L_{ex} during which this coupling is nonnegligible. The coupling is a reversible process, and the distance L_{ex} is optimized to maximize efficiency of ending up with a single photon in the waveguide (i.e., to prevent further Rabi oscillations back into the nanowire). A similar setup with a nanotip is illustrated in Fig. 1(c). Here, the nanotip radius $\rho(z)$ expands to some final radius R, at which point coupling with the waveguide starts to occur. Initiating the coupling once the nanotip has reached a constant radius allows the two systems to be easily mode matched, as discussed below. When optimized, we estimate that single-photon generation efficiencies exceeding ~95% are possible in this tiered configuration.

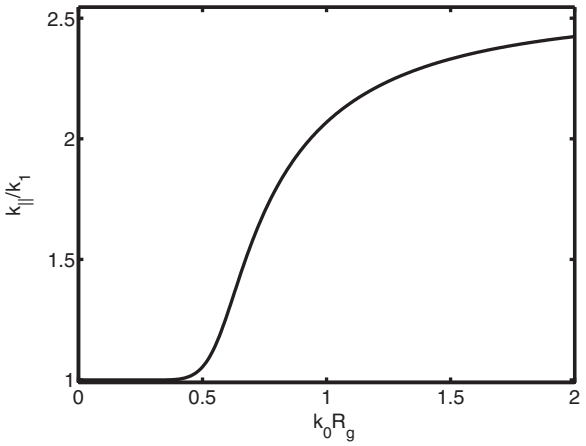

FIG. 6. Wave vector $k_{\|}$ of the fundamental guided modes of a cylindrical dielectric waveguide with core permittivity $\epsilon_c=13$ and surrounding permittivity $\epsilon_1=2$, plotted as a function of core radius R_g.

To treat the problem analytically, we consider the simple situation of our nanostructure coupled to a cylindrical dielectric waveguide (e.g, an optical fiber) of radius R_g, such that the modes can be calculated analytically using the methods described in Appendix A. It can be shown that the fundamental modes of the waveguide are degenerate $m=\pm 1$ modes that are not cut off as $R_g \to 0$. The dependence of their wave vector $k_{\|}$ on R_g is shown in Fig. 6 for a core permittivity $\epsilon_g=13$ and surrounding permittivity $\epsilon_1=2$. These parameters correspond closely to that of a Si/SiO_2 guide at $\lambda_0=1$ μm. To simplify the calculation, we also assume that coupling between the wire and higher-order waveguide modes is negligible. This can be achieved, for example, by operating below the cutoff radius of higher-order modes or by operating with sufficiently large wave vector mismatch between the plasmon and higher-order guide modes.

We make the ansatz that the total field of the system is given by a superposition of the unperturbed modes of the nanostructure and waveguide. While this cannot strictly be correct, as such a solution violates boundary conditions at each interface, we rely on such an assumption to give us the correct qualitative behavior without resorting to more complex numerical calculations. Specifically, we assume that the total electric field for the system takes the form

$$\mathbf{E}_T(\mathbf{r}) = \sum_{\mu=w,g} \sum_{i=1}^{N_\mu} C_{\mu,i}(z)\mathbf{E}_{\mu,i}(\mathbf{r}), \tag{50}$$

where μ indexes the nanostructure (w) and waveguide (g) systems, and $i=1,\ldots,N_\mu$ runs over the modes of system μ. In the following, we will explicitly treat the nanotip case, where the plasmons propagate in a single direction, although this argument can easily be extended to the nanowire. We emphasize that we are considering coupling of the plasmon mode to the waveguide once the nanotip has already ex-

panded to its final radius R, at which point the plasmon mode solution becomes identical to that of a nanowire. In our case, $N_w=1$ as we only consider the fundamental plasmon mode of the nanotip, while $N_g=2$ as we take into account the two degenerate, copropagating fundamental modes of the waveguide. $\mathbf{E}_{\mu,i}(\mathbf{r})$ here represents the unperturbed solution of mode i in system μ (without the presence of the other system). A similar expression holds for the total magnetic field.

With the ansatz of Eq. (50) for the total field of the combined waveguide and nanotip system, one can derive exact equations of evolution[46] based on Lorentz reciprocity for the coefficients $C_{\mu,i}$. Explicitly separating out the plane-wave dependence of the unperturbed fields, $\mathbf{E}_{\mu,i}(\mathbf{r})=\mathbf{E}_{\mu,i}(\boldsymbol{\rho})e^{ik_{\|\mu,i}z}$, the N_w+N_g coupled-mode equations take the form

$$\sum_{\nu=w,g}\sum_{j=1}^{N_\nu} P_{\mu,i;\nu,j}(z)\frac{dC_{\nu,j}}{dz} = i\omega\epsilon_0 \sum_{\nu=w,g}\sum_{j=1}^{N_\nu} K_{\mu,i;\nu,j}(z)C_{\nu,j}(z), \tag{51}$$

as derived in detail in Appendix E. The coefficients to the system of equations above are given by

$$P_{\mu,i;\nu,j}(z) = e^{i(k_{\|\nu,j}-k^*_{\|\mu,i})z}\int d\boldsymbol{\rho}[\mathbf{E}_{\nu,j}(\boldsymbol{\rho})\times\mathbf{H}^*_{\mu,i}(\boldsymbol{\rho}) + \mathbf{E}^*_{\mu,i}(\boldsymbol{\rho})\times\mathbf{H}_{\nu,j}(\boldsymbol{\rho})]\cdot\hat{z}, \tag{52}$$

$$K_{\mu,i;\nu,j}(z) = e^{i(k_{\|\nu,j}-k^*_{\|\mu,i})z}\int d\boldsymbol{\rho}\mathbf{E}_{\nu,j}(\boldsymbol{\rho})\cdot\mathbf{E}^*_{\mu,i}(\boldsymbol{\rho})[\epsilon_T(\boldsymbol{\rho})-\epsilon_\nu(\boldsymbol{\rho})], \tag{53}$$

where $\epsilon_T(\boldsymbol{\rho})$ is the electric permittivity of the combined system. Clearly, the presence of the phase factors $e^{i(k_{\|\nu,j}-k^*_{\|\mu,i})z}$ in the equations above indicates that, at least under weak coupling, significant power transfer between the two systems will not take place unless the two systems are approximately mode matched with respect to $k_\|$. In practice, this implies that for a final tip radius R, there is some ideal waveguide size R_g that allows for maximum transfer efficiency between the two systems. A similar optimization of the waveguide parameters exists in the case of arbitrary coupling strength between the two systems, although this problem is more complex because one must account for factors such as the phase shift of one system due to the other. We emphasize that the coupled-mode equations above are exact within the ansatz of Eq. (50). For example, for two lossless systems, these equations conserve power, and for a lossy system (such as a nanotip), the effects of losses are treated exactly. By convention, the normalization of fields is such that the integrals appearing in the diagonal matrix elements $P_{\mu,i;\mu,i}$ are set to 1.

For the waveguide and nanotip systems coupled over a length L_{ex}, the exact single-photon generation efficiency will depend on the details of how the two systems are brought together and separated apart. In practice, for example, the two systems should be brought together slowly enough that the introduction of the waveguide does not cause significant backscattering of the plasmon, yet quickly enough that this introduction length is small compared to the plasmon decay length. Furthermore, in reality, the coupling region will not be a step of length L_{ex}, but will be characterized by some smooth transition. To avoid the many details associated with this introduction and separation and to approximately calculate the efficiency, we will consider an idealized system and make three assumptions as follows:

(i) The decay rates of the emitter are not affected by the presence of the nearby dielectric waveguide. In particular, the Purcell factors calculated earlier for the nanotip are unchanged.

(ii) The radius of the nanotip is given by $\rho(z)=\sqrt{wz}$ for $z<z_0$ and becomes constant, $R\equiv\rho(z_0)=\sqrt{wz_0}$, for $z\geqslant z_0$. For $z\geqslant z_0$, the plasmon mode solution becomes identical to the nanowire solution, and in particular, has well-defined $k_\|$, which allows it to be easily mode matched with the waveguide. It is assumed that coupling between the nanotip and waveguide begins at $z=z_0$, with the initial field amplitudes of the coupled system given by

$$C_w(z_0) = \left[\frac{\tilde{P}(R)}{1+\tilde{P}(R)}\right]^{1/2}, \tag{54}$$

$$C_{g,i}(z_0) = 0, \tag{55}$$

where the probability $\tilde{P}(R)/[1+\tilde{P}(R)]$ of finding a plasmon excitation at R is already optimized over the nanotip curvature and emitter position.

(iii) Equation (51) exactly describes the coupling between the two systems in the region $z_0\leqslant z\leqslant z_0+L_{ex}$. To estimate the probability of transfer from nanowire to waveguide after distance L_{ex} when the two systems are once again separated, we project the total field of Eq. (50) at $z=z_0+L_{ex}$ into the waveguide mode. Specifically, the projected field amplitude in the waveguide in either of the degenerate modes i is given by

$$C_{\mathrm{proj},i}(z_0+L_{ex}) = 2\int d\boldsymbol{\rho}[\mathbf{E}_T(\mathbf{r})\times\mathbf{H}^*_{g,i}(\mathbf{r})]\cdot\hat{z}, \tag{56}$$

where the factor of 2 arises due to the normalization convention for the unperturbed modes.

Because of the symmetry, the projected field strengths $|C_{\mathrm{proj},i}|^2$ calculated above are equal for the two degenerate waveguide modes, and the quantity $2|C_{\mathrm{proj},i}|^2$ then corresponds to the efficiency of single-photon generation. Here, the additional factor of 2 accounts for the mode degeneracy. This quantity takes completely into account the propagative losses of the plasmons, imperfect coupling between the nanotip and waveguide, and the Purcell factor of the nanotip.

In Fig. 7(a), we plot the efficiency of single-photon generation as a function of R for both the nanowire and nanotip systems. For each R, the plotted efficiencies have been optimized over all other possible parameters of the system. For the nanowire configuration, we have assumed that the resulting forward- and backward-propagating waves in the waveguide can be perfectly combined. In the figure, we have also included points obtained by our BEM simulations of a nanotip. Here, we have taken the numerically optimized values of $\tilde{P}(R)$ and plugged them in as initial values for the coupled-mode theory above. It can be seen that the numerical simulations agree well with our theoretical predictions.

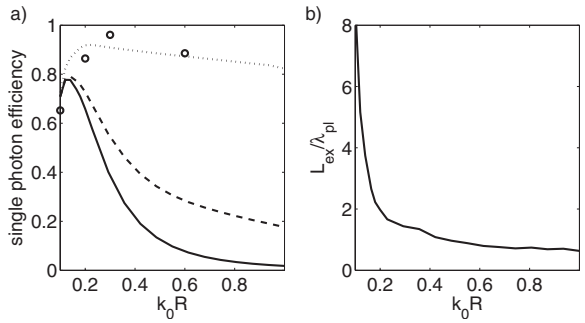

FIG. 7. (a) Optimized efficiencies of single-photon generation vs R. We have assumed that coupling to waveguide modes other than the fundamental mode is negligible, i.e., the waveguide is effectively in the single-mode regime. Solid (dashed) line: theoretical efficiency using a nanowire, using spontaneous emission rates obtained by quasistatic (fully electrodynamic) calculations. Dotted line: theoretical efficiency using a nanotip. Solid points: nanotip efficiency based on boundary element method simulations, combined with coupled-mode equations. (b) Optimal coupling length L_{ex} for a nanotip as a function of R. Here, L_{ex} is given in units of the plasmon wavelength λ_{pl} at that particular R.

We find that photon efficiencies of nearly 80% are possible for the nanowire,[37] while efficiencies exceeding 95% are possible for the nanotip. In Fig. 7(b), we plot the optimal coupling length L_{ex}, in units of λ_{pl}, as a function of R for the nanotip (L_{ex} for the nanowire should be twice that of the nanotip to account for the transfer of the forward- and backward-propagating components of the emitted plasmon). It can be seen that the outcoupling to the waveguide can, in principle, occur quite rapidly, over length scales of a few λ_{pl}.

The existence of an optimum R for photon generation can be intuitively understood. For smaller R, the coupling between the emitter and plasmon modes can be quite large. However, these tightly confined plasmon modes are accompanied by higher propagative losses and cannot be as efficiently coupled to the waveguide system. The coupling efficiency between plasmons and waveguide modes improves for larger R. For the nanowire, however, the larger radius results in weaker coupling between the plasmon and emitter, while for the nanotip, the accumulated propagative loss increases as the final radius grows.

VI. EFFECTS OF SURFACE ROUGHNESS

In previous sections, we have treated the problem of plasmon propagation on smooth nanowires and nanotips, taking into account inherent dissipative losses characterized by Im ϵ_2. In practice, however, these structures are not perfectly smooth and the surface roughness can give rise to new scattering mechanisms for the plasmons. While the general solution for the fields in the presence of arbitrary roughness is a complicated problem, we calculate the effects in two limits. In Sec. VI A, we calculate the losses on a nanowire due to radiative scattering in the limit of small roughness and zero heating (Im $\epsilon_2=0$). Here, the plasmons experience no inherent loss due to the metal but can receive momentum kicks from the roughness that cause them to scatter radiatively. In Sec. VI B, we calculate the effects of small roughness for a nanowire in the nonretarded limit, where radiative effects are ignored but the effects of increased dissipative losses are treated. While we explicitly treat only the nanowire case here, we note that the results obtained can also be incorporated into our model for nanotip losses via Eq. (49).

A. Radiative losses

For simplicity, we consider a wire with axial symmetry, but with a surface profile given by $\rho_0(z)=R+p\zeta(z)$, where R is the average radius of the wire, $\zeta(z)$ is some random function describing the roughness, and p is an expansion parameter that will be taken to equal 1 at the end. We will calculate in perturbation theory the radiated field scattered from the roughness, from an initial field corresponding to the fundamental plasmon mode for a perfectly smooth wire. Because of the symmetry, the only nonzero components of the fields remain, E_ρ, E_z, and H_ϕ, which will also have axial symmetry. As will be seen later, it suffices for now to consider only E_z, as the other components depend on E_z in a simple way through Maxwell's equations. We proceed by breaking up the total field along z in region i into incident and scattered fields

$$E_{i,z}^{\mathrm{total}} = E_{i,z}^{0} + E_{i,z}^{s}, \tag{57}$$

where $E_{i,z}^{0}$ is the z component of the fundamental plasmon mode given by Eqs. (3) and (4), and further assume that the scattered field can be expanded in a power series

$$E_{i,z}^{s} = \sum_{n=1}^{\infty} p^n E_{i,z}^{(n)}. \tag{58}$$

In the following, we will calculate the first-order scattered field $E_{i,z}^{(1)}$. We make the ansatz that $E_{i,z}^{(1)}$ can be expanded in the form[47]

$$E_{1,z}^{(1)} = \int_{-\infty}^{\infty} dh_{\parallel} H_0(h_{1\perp}\rho)\frac{h_{1\perp}^2}{k_1^2}A(h_{\parallel})e^{ih_{\parallel}z},$$

$$E_{2,z}^{(1)} = \int_{-\infty}^{\infty} dh_{\parallel} J_0(h_{2\perp}\rho)\frac{h_{2\perp}^2}{k_2^2}B(h_{\parallel})e^{ih_{\parallel}z}, \tag{59}$$

where each Fourier component is an outgoing solution of the wave equation with appropriate boundary conditions at $\rho=0$ and $\rho=\infty$, as derived in Eq. (A4). From Eq. (A4), one also sees that E_ρ and H_ϕ are determined completely once E_z is known. Using these relations, the total (incident plus scattered) fields $\mathbf{E}^{\mathrm{total}}$ and $\mathbf{H}^{\mathrm{total}}$ are straightforward but lengthy to write down, and are given to order p in Eq. (F1) in Appendix F.

The coefficients $A(h_{\parallel})$ and $B(h_{\parallel})$ are determined by enforcing continuity of the tangential fields at the boundary $\rho_0(z)$. Specifically, we require that

$$(\hat{t}\cdot\mathbf{E}_1^{\mathrm{total}})\big|_{\rho=R+p\zeta(z)} = (\hat{t}\cdot\mathbf{E}_2^{\mathrm{total}})\big|_{\rho=R+p\zeta(z)},$$

$$\hat{t} = \frac{\hat{z}+p\dfrac{d\zeta}{dz}\hat{\rho}}{\sqrt{1+p^2\left(\dfrac{d\zeta}{dz}\right)^2}},$$

$$H_{\phi,1}^{\text{total}}|_{\rho=R+p\zeta(z)} = H_{\phi,2}^{\text{total}}|_{\rho=R+p\zeta(z)}, \tag{60}$$

where $\hat{t}(z)$ is the unit tangent vector to the interface. These equations can be solved perturbatively by expanding them in p and solving each order. The $\mathcal{O}(p^0)$ equation is trivially satisfied by the fundamental plasmon mode for a smooth nanowire. To solve to $\mathcal{O}(p)$, it is useful to first introduce the Fourier transform of the surface roughness,

$$\zeta(z) = \int_{-\infty}^{\infty} \frac{dh_\parallel}{2\pi} e^{ih_\parallel z} \tilde{\zeta}(h_\parallel). \tag{61}$$

Using the Fourier transform $\tilde{\zeta}(h_\parallel)$, the $\mathcal{O}(p)$ equations become algebraic in Fourier space and have solutions (see Appendix F)

$$A(h_\parallel) = \frac{\tilde{\zeta}(h_\parallel - k_\parallel)}{2\pi} \frac{k_1^2}{h_{1\perp}} f(h_\parallel),$$

$$B(h_\parallel) = \frac{\tilde{\zeta}(h_\parallel - k_\parallel)}{2\pi} \frac{k_2^2}{h_{2\perp}} g(h_\parallel), \tag{62}$$

where $k_\parallel$ denotes the unperturbed plasmon wave vector (in this section, we take $\text{Im}\,\epsilon_2 = 0$ so that $k_\parallel$ is purely real). The scattering coefficients $f(h_\parallel)$ and $g(h_\parallel)$ are complicated functions of $h_\parallel$ and R, and are given in Appendix F. Physically, the equations above state that, to first order, the surface roughness contributes single momentum kicks to the unperturbed plasmon fields with a strength determined by the Fourier components of the roughness. From this point forward, we set $p=1$.

We now consider some random surface profile such that

$$\langle \zeta(z) \rangle = 0,$$

$$\langle \zeta(z)\zeta(z') \rangle = \delta^2 e^{-(z-z')^2/a^2}, \tag{63}$$

with corresponding correlations

$$\langle \tilde{\zeta}(k) \rangle = 0,$$

$$\langle \tilde{\zeta}(k)\tilde{\zeta}^*(k') \rangle = 2\pi^{3/2}\delta^2 a e^{-(1/4)a^2k^2}\delta(k-k'), \tag{64}$$

for the Fourier components. Physically, δ and a correspond respectively to the typical amplitude and length of a rough patch on the surface of the wire. It is also useful to define $s=\delta/a$ as a typical "slope" to the roughness. To calculate the power radiated due to the surface roughness, we find the ensemble-averaged Poynting vector far from the wire. It is sufficient to consider just the component of $\langle \mathbf{S} \rangle$ oriented along $\hat{\rho}$, given outside the wire by

$$S_\rho = -\frac{1}{2}\langle E_{1,z}^{\text{total}} H_{1,\phi}^{*\text{total}} \rangle, \tag{65}$$

where the fields $E_{1,z}^{\text{total}}$ and $H_{1,\phi}^{\text{total}}$ are given to first order by Eq. (F1). The calculation of S_ρ simplifies further because the incident plasmon field decays exponentially away from the wire, and thus, to lowest order only the first-order scattered fields will contribute to the Poynting vector at large ρ, which physically corresponds to the power radiated away to infinity. Specifically, the radiated power per unit area is given by

$$S_\rho = -\frac{1}{2}\langle E_{1,z}^{(1)} H_{1,\phi}^{(1)*} \rangle \quad (\rho \to \infty) \tag{66a}$$

$$= \frac{1}{2\omega\mu_0}\int_{-\infty}^{\infty} dh_\parallel dh_\parallel' \frac{ih_{1\perp}{}^2 h_{1\perp}'^*}{k_1^2} H_0(h_{1\perp}\rho) H_0'^*(h_{1\perp}'\rho)$$
$$\times \langle A(h_\parallel) A^*(h_\parallel') \rangle e^{i(h_\parallel - h_\parallel')z}. \tag{66b}$$

Substituting the solution for $A(h_\parallel)$ derived in Eq. (62) and using the correlations in Eq. (64), it is straightforward to evaluate the integral over $h_\parallel'$ and arrive at

$$S_\rho = \frac{i\epsilon_0\epsilon_1\omega}{4\sqrt{\pi}} s^2 a^3 \int_{-k_1}^{k_1} dh_\parallel e^{-(1/4)a^2(h_\parallel - k_\parallel)^2} h_{1\perp}$$
$$\times H_0(h_{1\perp}\rho) H_0'^*(h_{1\perp}\rho) |f(h_\parallel)|^2. \tag{67}$$

In the expression above, we have truncated the bounds of the integral to $\pm k_1$ because we are interested in the Poynting vector far away from the wire, where only radiative fields $|h_\parallel| \leqslant k_1$ contribute. With knowledge of the Poynting vector, it is then possible to find the dissipation rate of the plasmons due to radiative scattering, given by

$$\Gamma_{\text{rad,rough}} = \lim_{\rho\to\infty} \frac{2\pi\rho S_\rho}{\frac{1}{4}\int d\boldsymbol{\rho}\epsilon_0 \frac{d}{d\omega}[\epsilon(\boldsymbol{\rho},\omega)\omega]|\mathbf{E}(\boldsymbol{\rho})|^2 + \mu_0|\mathbf{H}(\boldsymbol{\rho})|^2}. \tag{68}$$

The denominator on the right-hand side of the equation above can be identified with the plasmon energy per unit length.

We first qualitatively discuss the behavior of $\Gamma_{\text{rad,rough}}$ before deriving various limits more quantitatively. From Eq. (67), it is clear that $\Gamma_{\text{rad,rough}}$ scales explicitly like δ^2 or s^2. Physically, this occurs because the lowest-order contribution to the Poynting vector far away from the wire is due to the combination of a first-order scattered electric field and first-order scattered magnetic field. In Fig. 8, the quantity $\Gamma_{\text{rad,rough}}/s^2\omega$ is evaluated numerically as a function of wire radius R and correlation length a/R for a silver nanowire at $\lambda_0 = 1\ \mu$m and $\epsilon_1 = 2$. We are particularly interested in the nanowire limit, when the plasmon wave vector $k_\parallel \approx C/R$. We see that for fixed R, the scattering reaches a peak for some particular value of a/R. More careful inspection reveals that the maximum occurs when $a \propto R/C \propto \lambda_{\text{pl}}$. This result makes intuitive sense, since the characteristic momentum kick $\sim 1/a$ that the plasmon wave vector $k_\parallel$ receives due to roughness must be on the order of C/R in order for the resulting wave vector to lie in the radiative range between $-k_1$ and k_1. In the limit $a/R \gg C$, one observes an exponential suppression of scattering, due to the fact that the roughness has a very narrow momentum distribution and cannot possibly contribute a large kick to $k_\parallel$. In fact, in this regime, one physically expects the plasmon wave vector to adiabatically vary with the changing wire radius. In the other limit $a/R \ll C$, the scattering also decreases, but with a polynomial

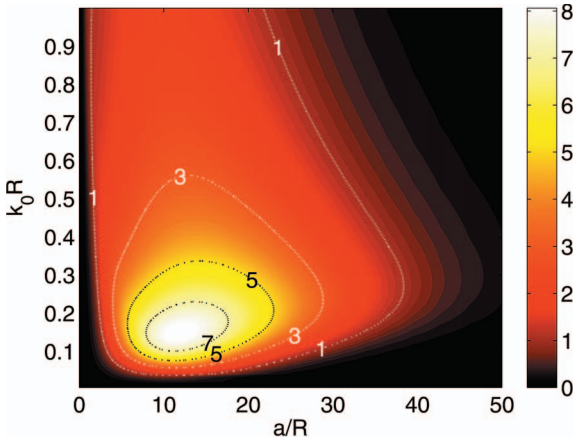

FIG. 8. (Color online) The plasmon dissipation rate due to radiative scattering off of surface roughness, $\Gamma_{\mathrm{rad,rough}}/s^2\omega$, as functions of wire radius R and correlation length a/R. The numbers are calculated for a silver nanowire at $\lambda_0=1$ μm and $\epsilon_1=2$.

dependence on R, as will be proven below. Here, the momentum distribution of the roughness becomes very wide, and thus, the probability of receiving a kick that results in a final momentum between $\pm k_1$ becomes quite small. Finally, for fixed slope s, it can be seen that the scattering decreases as $R\to 0$ at any correlation length a. This result is also easily understood, as the plasmon wave vector $k_\parallel$ becomes increasingly far removed from the range of radiative wave vectors. In Table I, we calculate the scattering rates for wire sizes $k_0R=0.1$, 0.2, and 0.3 (or $R\approx 16$, 32, and 48 nm), for a few chosen roughness parameters. The scattering rates are given as a percentage increase in Im $k_\parallel$ over the values for a smooth nanowire. It can be seen that strong suppression of radiative scattering occurs both for smaller R and when a is either much larger or much smaller than R, which confirms our earlier observations. Furthermore, it is evident that under reasonable parameters, the losses in the system are increased only slightly due to radiative scattering.

We now analyze more carefully the behavior of the radiative scattering in the nanowire regime. To simplify the expression further, we first note that since we are interested in the far field ($\rho\to\infty$), we can take the asymptotic limits of the Hankel functions in Eq. (67), $H_0(h_{1\perp}\rho)H_0'^{*}(h_{1\perp}\rho)\approx -2i/(\pi h_{1\perp}\rho)$. One can also derive an asymptotic relationship of $f(h_\parallel)$ as $R\to 0$ (see Appendix F), which upon substitution yields

$$\Gamma_{\mathrm{rad,rough}} \approx \pi^{3/2}\frac{|\phi|^2}{\tilde{V}}\omega\epsilon_1 s^2 a^3 \int_{-k_1}^{k_1} dh_\parallel h_{1\perp}^2 e^{-(1/4)a^2(k_\parallel - h_\parallel)^2} \quad (R\to 0), \tag{69}$$

$$\phi \equiv \frac{H_0'(iC)}{J_0'(iC)}J_0''(iC) - H_0''(iC). \tag{70}$$

Here, $\tilde{V}$ is a complicated dimensionless parameter, but most importantly, only depends on $\epsilon_{1,2}$.

From the equation above, it is clear that there are three distinct regimes of interest defined by the quantity $\alpha\equiv k_\parallel a = 2\pi a/\lambda_{\mathrm{pl}}\approx Ca/R$, which characterizes the typical extent of a rough patch compared to the plasmon wavelength. In the limit $\alpha\ll 1$, one can approximate the exponential in the integrand of Eq. (69) as a constant, which leads to straightforward evaluation of the integral,

$$\Gamma_{\mathrm{rad,rough}} \approx \frac{4}{3}\pi^{3/2}\frac{|\phi|^2}{\tilde{V}}\omega\epsilon_1^{5/2}s^2\left(\frac{k_0R}{C}\right)^3\alpha^3 \quad (\alpha\ll 1). \tag{71}$$

Here, the noise spectrum of Eq. (64) becomes very wide and leads to an α^3 scaling of the dissipation rate. In the opposite limit $\alpha\gg 1$, the value of the exponential term becomes exponentially small, with a corresponding exponential suppression of the scattering rate. A more careful evaluation of the integrand yields

$$\Gamma_{\mathrm{rad,rough}} \approx 8\pi^{3/2}\frac{|\phi|^2}{\tilde{V}}\omega\epsilon_1^{3/2}s^2\frac{k_0R}{C\alpha}e^{-(1/4)a^2(k_\parallel - k_1)^2} \quad (\alpha\gg 1). \tag{72}$$

Finally, one can show that for fixed, subwavelength R, the radiative scattering is most significant when $\alpha\sim\mathcal{O}(1)$. In this case, the exponential appearing in Eq. (69) is neither exponentially small nor constant. However, one can make the rough approximation $e^{-(1/4)a^2(k_\parallel - h_\parallel)^2}\approx 1-(1/4)a^2(k_\parallel - h_\parallel)^2$ to get an idea of the scaling in this regime. It is straightforward to show that the scattering rate has a maximum with respect

TABLE I. Losses due to radiative scattering off of surface roughness for nanowires of varying sizes and roughness parameters. The scattering rates are given in terms of the percentage increase in Im $k_\parallel$ that one would expect over the values for a smooth nanowire.

Roughness parameters	$k_0R=0.1$ ($R\approx 16$ nm)	$k_0R=0.2$ ($R\approx 32$ nm)	$k_0R=0.3$ ($R\approx 48$ nm)
$a=0.1R$, $\delta=0.05R$ ($s=0.5$)	0.09%	0.5%	1.4%
$a=0.1R$, $\delta=0.1R$ ($s=1$)	0.4%	1.9%	5.6%
$a=R$, $\delta=0.05R$ ($s=0.05$)	0.9%	4.5%	12%
$a=5R$, $\delta=0.05R$ ($s=0.01$)	2.8%	8.0%	10%
$a=10R$, $\delta=0.1R$ ($s=0.01$)	7.0%	14%	16%
$a=20R$, $\delta=0.1R$ ($s=0.005$)	0.9%	2.9%	3.8%
$a=25R$, $\delta=0.1R$ ($s=0.004$)	0.3%	1.3%	1.8%

to α at $\alpha \approx (12/5)^{1/2}$, with a corresponding maximum decay rate

$$\max_a\{\Gamma_{\mathrm{rad,rough}}\} \propto \frac{|\phi|^2}{\tilde{V}}\omega\epsilon_1^{5/2}s^2\left(\frac{k_0R}{C}\right)^3. \tag{73}$$

Again, the radiative scattering is most significant when the length scale a of the roughness is on the order of the plasmon wavelength, and the maximum scattering (for fixed s) decreases as $R\to 0$ due to the increasing mismatch between $k_\parallel$ and radiative wave vectors.

We now consider the limits of validity of the derivations above, specifically considering the expansions made in Eq. (F2) that are necessary for the perturbative method used here. The first of these expansions requires that $|d\zeta/dz| \ll 1$, which can be rewritten as a condition on the slope, $s \ll 1$. Physically, this requirement states that the typical length of a rough patch be much larger than its typical height. The second line of Eq. (F2) requires that $|k_{i\perp}\zeta| \ll 1$. In the nanowire regime, this requirement is equivalent to $\delta \ll \lambda_{\mathrm{pl}}$, which states that the height of a rough patch must be much smaller than the plasmon wavelength. Finally, the third line of Eq. (F2) requires $|h_{i\perp}\zeta| \ll 1$, within the range of $h_{i\perp}$ that are appreciably scattered into. From Eqs. (62) and (64), we see that the relevant range for the parallel component of the wave vector is given by $k_\parallel - 1/a \lesssim h_\parallel \lesssim k_\parallel + 1/a$, and thus, the largest relevant transverse wave vector is $|h_{i\perp,\max}| \sim \max_{-1\le\theta\le 1}|\sqrt{\epsilon_i(\omega/c)^2-(k_\parallel+\theta/a)^2}|$. In the nanowire regime, $k_\parallel \approx C/R$, there are two limiting cases. The first is when the correlation length a is much larger than R, $a \gg R$, in which case $|h_{i\perp,\max}| \sim C/R$ and $|h_{i\perp}\zeta| \ll 1$ reduces to $\delta \ll \lambda_{\mathrm{pl}}$. In the other limiting case, $R \gg a$, one finds that $|h_{i\perp,\max}| \sim 1/a$ and the corresponding requirement is given by $s \ll 1$.

We finally note that while the radiative scattering goes like δ^2 or s^2, the relevant quantity for dissipative (heating) losses due to roughness becomes $\mathbf{S}$ inside the wire. For this quantity, the lowest-order correction to the smooth wire solution will come from a combination of a first-order and zeroth-order field. Thus one expects roughness-induced dissipative losses to contribute a decay term proportional to δ or s, which for small roughness will dominate over radiative scattering. This correction will be treated in the next section.

B. Nonradiative losses

To study the effects of surface roughness on nonradiative losses, we will make one simplifying assumption and calculate these losses in the quasistatic limit. To do this, we will proceed in a manner similar to that in Sec. III A, where we found the quasistatic fields associated with a smooth nanowire. Here, the calculations for the fields yielded the presence of poles whose positions and widths give the real and imaginary parts of the wave vector $k_\parallel$. The case of a smooth nanowire was particularly easy to treat because of the translational symmetry of the system. A system containing surface roughness lacks such translational symmetry, and therefore, must be considered more carefully, but the calculation proceeds in much the same way. In particular, we will find expressions for the pseudopotentials $\Phi_1 = \Phi_0 + \Phi_r$ and Φ_2 that satisfy the necessary boundary conditions in the presence of surface roughness. We can once again find the positions and widths of the poles associated with the system, which are now altered by the roughness.

We first write down appropriate expansions for $\Phi_{0,r,2}(\mathbf{r},\mathbf{r}')$. The expansion for the incident component Φ_0, given originally in Eq. (11), is slightly rewritten here,

$$\begin{aligned}\Phi_0(\mathbf{r},\mathbf{r}') &= \frac{1}{4\pi\epsilon_0\epsilon_1}\frac{1}{|\mathbf{r}-\mathbf{r}'|}\\ &= \frac{1}{2\pi^2\epsilon_0\epsilon_1}\sum_{m=0}^{\infty}(2-\delta_{m,0})\cos[m(\phi-\phi')]\\ &\quad\times\int_0^\infty dh\,\cos[h(z-z')]K_m(h\rho')I_m(h\rho)\quad(\rho<\rho')\\ &= \frac{1}{4\pi^2\epsilon_0\epsilon_1}\sum_{m=-\infty}^{\infty}e^{im(\phi-\phi')}\int_{-\infty}^{\infty}dh e^{ih(z-z')}\\ &\quad\times\tilde{K}_m(h\rho')\tilde{I}_m(h\rho)\quad(\rho<\rho').\end{aligned} \tag{74}$$

The functions $\tilde{K}_m(x), \tilde{I}_m(x)$ are defined by

$$\tilde{K}_m, \tilde{I}_m(x) = K_m, I_m(|x|). \tag{75}$$

We also break up $\Phi_{r,2}$ into Fourier components that satisfy Laplace's equation and assume that these expressions hold up to the interface:

$$\Phi_r(\mathbf{r},\mathbf{r}') = \frac{1}{4\pi^2\epsilon_0\epsilon_1}\sum_{m=-\infty}^{\infty}e^{im(\phi-\phi')}\int_{-\infty}^{\infty}dh e^{ih(z-z')}\tilde{K}_m(h\rho)\alpha_m(h), \tag{76}$$

$$\Phi_2(\mathbf{r},\mathbf{r}') = \frac{1}{4\pi^2\epsilon_0\epsilon_1}\sum_{m=-\infty}^{\infty}e^{im(\phi-\phi')}\int_{-\infty}^{\infty}dh e^{ih(z-z')}\tilde{I}_m(h\rho)\beta_m(h). \tag{77}$$

To describe the surface roughness, we assume an interface with axial symmetry as before, $\rho_0(z) = R + p\zeta(z)$, where the roughness profile ζ satisfies the correlations given in Eqs. (63) and (64). The coefficients α_m and β_m are determined by the boundary conditions, namely, that Φ and $\mathbf{D}_\perp$ must be continuous at the interface:

$$\Phi_1(\mathbf{r},\mathbf{r}')|_{\rho=R+p\zeta(z)} = \Phi_2(\mathbf{r},\mathbf{r}')|_{\rho=R+p\zeta(z)},$$

$$\epsilon_1\hat{n}\cdot\nabla\Phi_1(\mathbf{r},\mathbf{r}')|_{\rho=R+p\zeta(z)} = \epsilon_2\hat{n}\cdot\nabla\Phi_2(\mathbf{r},\mathbf{r}')|_{\rho=R+p\zeta(z)},$$

$$\hat{n} = \frac{\hat{\rho} - p\dfrac{d\zeta}{dz}\hat{z}}{\sqrt{1+p^2\left(\dfrac{d\zeta}{dz}\right)^2}}. \tag{78}$$

Plugging in the expressions for Φ_i given by Eqs. (74), (76), and (77), one can expand both boundary condition equations to $\mathcal{O}(p^2)$. Then, replacing $\zeta(z)$ in these equations with its Fourier transform given in Eq. (61), one obtains a set of

coupled equations for α_m and $\beta_m(h)$ completely in Fourier space, which, unlike the case of a smooth nanowire, is not decoupled in h. It is tedious but straightforward to show that, to $\mathcal{O}(p^2)$, this set of equations is given by the matrix integral equation

$$M_0(h)\begin{pmatrix}\alpha_m(h)\\ \beta_m(h)\end{pmatrix} + p\int \frac{dq}{2\pi}\tilde{\zeta}(h-q)M_1(h,q)\begin{pmatrix}\alpha_m(q)\\ \beta_m(q)\end{pmatrix} + p^2\int \frac{dqdq'}{(2\pi)^2}\tilde{\zeta}(h-q-q')\tilde{\zeta}(q') \times M_2(h,q,q')\begin{pmatrix}\alpha_m(q)\\ \beta_m(q)\end{pmatrix} + \mathcal{O}(p^3) = \mathbf{v}_0(h) + p\int \frac{dq}{2\pi}\tilde{\zeta}(h-q)\mathbf{v}_1(h,q) + p^2\int \frac{dqdq'}{(2\pi)^2}\tilde{\zeta}(h-q-q')\tilde{\zeta}(q')\mathbf{v}_2(h,q,q') + \mathcal{O}(p^3). \tag{79}$$

The matrices M_i and vectors $\mathbf{v}_i$ are complicated expressions and are given in Appendix G. We note, however, that in the case of no surface roughness ($\tilde{\zeta}=0$), the solution to the resulting equation $M_0(h)\cdot[\alpha_m(h)\beta_m(h)]^T=\mathbf{v}_0(h)$ reduces to that of a smooth nanowire.

We now discuss how to solve Eq. (79) in the presence of surface roughness, using the methods detailed in Ref. 48. One might first consider expanding α_m and β_m in a power series of p, in a manner similar to the field expansion in Eq. (58) for the case of radiative scattering, and then solving the $\mathcal{O}(p^{n+1})$ equations based on the $\mathcal{O}(p^n)$ solutions. However, such a perturbative solution simply yields poles for each higher-order correction with the same location as that of the unperturbed solutions $\alpha_m^{(0)}$ and $\beta_m^{(0)}$. Mathematically, this occurs because each calculation of the next correction involves an inversion $M_0^{-1}(h)$. On the other hand, physically, we expect for the surface roughness to result in some shift of the pole that is not predicted by such a perturbative method.[48] We thus consider an alternate approach, in which we symbolically sum the perturbation series in Eq. (79) to all orders and then only keep the lowest-order result in p. Let us symbolically write Eq. (79) in the form

$$(\mathcal{M}_0 + \delta\mathcal{M})\mathbf{x} = \mathbf{f}_0 + \delta\mathbf{f}, \tag{80}$$

where $\mathcal{M}_0$ and $\mathbf{f}_0$ are nonrandom matrices and vectors, respectively, $\delta\mathcal{M}$ is a random 2×2 matrix integral operator, $\delta\mathbf{f}$ is a random vector, and $\mathbf{x}$ is a column vector with components α_m and β_m. We now define the averaging operator

$$Px = \langle x\rangle, \tag{81}$$

and the operator $Q=1-P$. We can apply P and Q to Eq. (80) to get

$$P\mathcal{M}_0\mathbf{x} + P\delta\mathcal{M}\mathbf{x} = P(\mathbf{f}_0 + \delta\mathbf{f}), \tag{82}$$

$$Q\mathcal{M}_0\mathbf{x} + Q\delta\mathcal{M}\mathbf{x} = Q(\mathbf{f}_0 + \delta\mathbf{f}), \tag{83}$$

which after some manipulation results in the set of equations

$$(\mathcal{M}_0 + P\delta\mathcal{M})\langle\mathbf{x}\rangle + P\delta\mathcal{M}Q\mathbf{x} = P(\mathbf{f}_0 + \delta\mathbf{f}), \tag{84}$$

$$Q\mathbf{x} = (1+\mathcal{M}_0^{-1}Q\delta\mathcal{M})^{-1}\mathcal{M}_0^{-1}Q(\mathbf{f}_0+\delta\mathbf{f}) - (1+\mathcal{M}_0^{-1}Q\delta\mathcal{M})^{-1}\mathcal{M}_0^{-1}Q\delta\mathcal{M}\langle\mathbf{x}\rangle. \tag{85}$$

One can then substitute Eq. (85) into Eq. (84) and solve for $\langle\mathbf{x}\rangle$, in which case one obtains

$$(\mathcal{M}_0 + \langle(1+\delta\mathcal{M}\mathcal{M}_0^{-1}Q)^{-1}\delta\mathcal{M}\rangle)\langle\mathbf{x}\rangle = \langle(1+\delta\mathcal{M}\mathcal{M}_0^{-1}Q)^{-1}(\mathbf{f}_0+\delta\mathbf{f})\rangle. \tag{86}$$

We note that, unlike a perturbative expansion and solution for α_m and β_m, the equation above is, thus far, exact. Now, we assume that $\delta\mathcal{M}$ and $\delta\mathbf{f}$ can be expanded in powers of p in the form

$$\delta\mathcal{M} = p\delta\mathcal{M}_1 + p^2\delta\mathcal{M}_2 + \cdots,$$

$$\delta\mathbf{f} = p\delta\mathbf{f}_1 + p^2\delta\mathbf{f}_2 + \cdots. \tag{87}$$

Comparing Eqs. (79) and (87), we see that $\langle\delta\mathcal{M}_1\rangle=\langle\delta\mathbf{f}_1\rangle=0$ since $\langle\tilde{\zeta}\rangle=0$. With this result, and utilizing the definition $Q=1-P$, one can proceed to expand Eq. (86) up to $\mathcal{O}(p^2)$, which yields (after setting $p=1$)

$$(\mathcal{M}_0 + \langle\delta\mathcal{M}_2\rangle - \langle\delta\mathcal{M}_1\mathcal{M}_0^{-1}\delta\mathcal{M}_1\rangle)\langle\mathbf{x}\rangle = \langle\mathbf{f}_0\rangle + \langle\delta\mathbf{f}_2\rangle - \langle\delta\mathcal{M}_1\mathcal{M}_0^{-1}\delta\mathbf{f}_1\rangle. \tag{88}$$

Substituting the corresponding terms of Eq. (79) into the equation above and using the second-order correlations given by Eq. (64), we find after simplifying that

$$\left\{M_0(h) + \frac{s^2a^3}{2\sqrt{\pi}}\int dq[e^{-a^2q^2/4}M_2(h,h,q) - e^{-a^2(h-q)^2/4}M_1(h,q)M_0^{-1}(q)M_1(q,h)]\right\}\begin{pmatrix}\alpha_m(h)\\ \beta_m(h)\end{pmatrix} = \left\{\mathbf{v}_0(h) + \frac{s^2a^3}{2\sqrt{\pi}}\int dq[e^{-a^2q^2/4}\mathbf{v}_2(h,h,q) - e^{-a^2(h-q)^2/4}M_1(h,q)M_0^{-1}(q)\mathbf{v}_1(q,h)]\right\}, \tag{89}$$

where $s=\delta/a$.

We now discuss the solution to $\alpha_0(h)$, which contains a pole corresponding to the fundamental plasmon mode $m=0$. When ϵ_2 is a negative real number, α_0 has a pole on the real h axis, whose position gives the new, shifted plasmon wave vector $\tilde{k}_\parallel$. When ϵ_2 has a nonzero imaginary component, α_0 will have a resonance feature along this axis, whose peak corresponds to Re $\tilde{k}_\parallel$ and whose width corresponds to Im $\tilde{k}_\parallel$. A quick inspection of the equation above reveals that $\tilde{k}_\parallel R=\tilde{C}(\epsilon_i,s,a/R)$ is a constant that depends only on the quantities ϵ_i, s, and a/R. Unfortunately, because of the complexity of Eq. (89), it is difficult to derive other scaling results for $\tilde{k}_\parallel$ even in limiting cases. However, Eq. (89) can be solved numerically. In practice, for known parameters, the matrices M and vectors $\mathbf{v}$ can be readily evaluated over some range of h,

TABLE II. Losses and wave vector shifts due to nonradiative scattering off of surface roughness for nanowires with varying roughness parameters. The shifts in Re $\tilde{C}$ and changes in loss parameters Im $\tilde{C}$/Re $\tilde{C}$ are given in terms of percentage increase over the corresponding values for a smooth nanowire.

Roughness parameters	Δ(Re $\tilde{C}$)	Δ(Im $\tilde{C}$/Re $\tilde{C}$)
$a=0.1R$, $\delta=0.01R$ ($s=0.1$)	0.2%	0.2%
$a=0.1R$, $\delta=0.05R$ ($s=0.5$)	7.5%	6.8%
$a=R$, $\delta=0.01R$ ($s=0.01$)	0.03%	1.0%
$a=R$, $\delta=0.05R$ ($s=0.05$)	0.9%	26%
$a=R$, $\delta=0.1R$ ($s=0.1$)	3.5%	110%
$a=10R$, $\delta=0.01R$ ($s=0.001$)	>0.01%	2.7%
$a=10R$, $\delta=0.05R$ ($s=0.005$)	0.2%	67%
$a=10R$, $\delta=0.1R$ ($s=0.01$)	0.8%	270%

from which the solutions to the systems α_0 and $\beta_0(h)$ in that range immediately follow. The resulting resonance in Im $\alpha_0(h)$ as a function of h is then fitted to a Lorentzian, with its peak giving the shifted wave vector Re $\tilde{k}_\parallel$ and its half-width giving Im $\tilde{k}_\parallel$. In Table II, we give the resulting losses and wave vector shifts for a few roughness parameters, as calculated through Eq. (89). Again the numbers that we have used are for a silver nanowire at $\lambda_0=1$ μm and $\epsilon_1=2$. The shifts in Re $\tilde{k}_\parallel$ (or equivalently, Re $\tilde{C}$) and increases in the loss parameter Im $\tilde{k}_\parallel$/Re $\tilde{k}_\parallel$ (or Im $\tilde{C}$/Re $\tilde{C}$) are given in terms of the percentage increase over their values for a smooth nanowire. Again it can be seen that for reasonable parameters, surface roughness adds only a moderate amount of loss to the system.

VII. CONCLUSIONS AND OUTLOOK

We have demonstrated that the subwavelength confinement of guided plasmon modes on conducting nanostructures leads to strong coupling between these modes and nearby emitters in the optical domain. This strong coupling leads to large effective Purcell factors for emission into the plasmon modes, which are limited only by heating losses in the conductor. While losses prevent the plasmon modes from being useful photonic carriers of information, we have shown that they can be efficiently outcoupled, e.g, to a dielectric waveguide. We estimate that single-photon generation efficiencies exceeding 95% are possible in such a tiered system. Finally, we have analyzed the effects of plasmon scattering due to moderate surface roughness on these nanostructures.

Rapid advances in recent years in fabrication techniques for nanowires,[49,50] nanotips,[51] and subwavelength dielectric waveguides[52,53] put such a system in experimental reach. Quantum dots or single color centers might serve as physical realizations of solid-state emitters, which could be used to achieve strong-coupling cavity QED and quantum information devices on a chip at optical frequencies. It is also interesting to consider real, individual atoms interacting with nanowires and the challenges associated with constructing nanoscale traps. These traps might in part be formed by the plasmon fields themselves.

We emphasize that the physical mechanisms that lead to strong coupling are not restricted to the nanostructures considered here but can be quite a general feature of the plasmon modes associated with subwavelength conducting devices. It is thus likely that the efficiencies calculated here are not fundamentally limited but can be further improved by proper design. Photonic crystal-like structures for plasmons,[54] for example, may be a promising approach to achieve tight confinement while simultaneously reducing losses. Similar schemes may also help to improve coupling between the plasmons and dielectric waveguide modes. Such approaches are likely to improve the performance of plasmon cavity QED even further.

ACKNOWLEDGMENTS

The authors thank Atac Imamoglu for useful discussions. This work was supported by the ARO-MURI, ARDA, NSF, the Sloan and Packard Foundations, and by the Danish Natural Science Research Council.

APPENDIX A: GENERAL THEORY OF ELECTROMAGNETIC MODES OF A CYLINDER

The solution to the electromagnetic modes of a cylinder has been known for quite some time[26,27] and is briefly derived here.

We consider a cylinder of radius R of dimensionless electric permittivity ϵ_2, centered along the z axis and surrounded by a second dielectric medium ϵ_1. For nonmagnetic media, the electric and magnetic fields in frequency space satisfy the wave equation

$$\nabla^2 \begin{Bmatrix} \mathbf{E}(\mathbf{r}) \\ \mathbf{H}(\mathbf{r}) \end{Bmatrix} + \frac{\omega^2}{c^2}\epsilon(\mathbf{r}) \begin{Bmatrix} \mathbf{E}(\mathbf{r}) \\ \mathbf{H}(\mathbf{r}) \end{Bmatrix} = 0. \tag{A1}$$

The solutions to Eq. (A1) are perhaps most easily derived by first finding scalar solutions of the equation and then constructing vector solutions. Working in cylindrical coordinates, scalar solutions of Eq. (A1) satisfying the necessary boundary conditions take the form $\psi_1 \propto H_m(k_{1\perp}\rho)e^{im\phi+ik_\parallel z}$ and $\psi_2 \propto J_m(k_{2\perp}\rho)e^{im\phi+ik_\parallel z}$ outside and inside the cylinder, respectively. Here, J_m and H_m are Bessel functions and Hankel functions of the first kind, respectively, while $k_{i\perp}=\sqrt{k_i^2-k_\parallel^2}$ and $k_i=\omega\sqrt{\epsilon_i}/c$. J_m is well behaved at $\rho=0$, while $H_m(x) \sim e^{ix}$ for large x satisfies outgoing-wave conditions. It is easy to verify that two independent vector solutions to Eq. (A1) are given by $\mathbf{v}_i=\frac{1}{k_i}\nabla\times(\hat{z}\psi_i)$ and $\mathbf{w}_i=\frac{1}{k_i}\nabla\times\mathbf{v}_i$. The curl relations of Maxwell's equations then imply that $\mathbf{E}$ and $\mathbf{H}$ must take the form

$$\mathbf{E}_i(\mathbf{r}) = a_i\mathbf{v}_i(\mathbf{r}) + b_i\mathbf{w}_i(\mathbf{r}), \tag{A2}$$

$$\mathbf{H}_i(\mathbf{r}) = -\frac{i}{\omega\mu_0}k_i[a_i\mathbf{w}_i(\mathbf{r}) + b_i\mathbf{v}_i(\mathbf{r})], \tag{A3}$$

where a_i and b_i are constant coefficients. Expanding out these expressions in detail,

$$\mathbf{E}_i(\mathbf{r}) = \left\{ \left[\frac{im}{k_i\rho} a_i F_{i,m}(k_{i\perp}\rho) + \frac{ik_\parallel k_{i\perp}}{k_i^2} b_i F'_{i,m}(k_{i\perp}\rho) \right] \hat{\rho} + \left[-\frac{k_{i\perp}}{k_i} a_i F'_{i,m}(k_{i\perp}\rho) - \frac{mk_\parallel}{k_i^2\rho} b_i F_{i,m}(k_{i\perp}\rho) \right] \hat{\phi} + \frac{k_{i\perp}^2}{k_i^2} b_i F_{i,m}(k_{i\perp}\rho)\hat{z} \right\} e^{im\phi + ik_\parallel z},$$

$$\mathbf{H}_i(\mathbf{r}) = -\frac{i}{\omega\mu_0} k_i \left\{ \left[\frac{ik_\parallel k_{i\perp}}{k_i^2} a_i F'_{i,m}(k_{i\perp}\rho) + \frac{im}{k_i\rho} b_i F_{i,m}(k_{i\perp}\rho) \right] \hat{\rho} - \left[\frac{mk_\parallel}{k_i^2\rho} a_i F_{i,m}(k_{i\perp}\rho) + \frac{k_{i\perp}}{k_i} b_i F'_{i,m}(k_{i\perp}\rho) \right] \hat{\phi} + \frac{k_{i\perp}^2}{k_i^2} a_i F_{i,m}(k_{i\perp}\rho)\hat{z} \right\} e^{im\phi + ik_\parallel z}, \tag{A4}$$

where $F_{1,m}(x)=H_m(x)$ and $F_{2,m}(x)=J_m(x)$.

Up to this point a_i and b_i are arbitrary coefficients, whose relationship becomes fixed by imposing boundary conditions between the cylinder and surrounding dielectric. Requiring that the tangential components E_ϕ, E_z, H_ϕ, and H_z of the fields be continuous at the boundary results in a linear system of four equations, which we write in abbreviated matrix form as $M(a_1\ a_2\ b_1\ b_2)^T=0$.[55] A nontrivial solution for the fields requires that $\det M=0$, which after some work simplifies to the mode equation given in Eq. (1).

One special case of interest is that of a TM mode with no winding ($m=0$). The component of $\mathbf{H}$ along $\hat{z}$ by definition vanishes, which implies that the coefficients a_i in Eq. (A4) vanish. The condition $\det M=0$ is then significantly easier to evaluate in this situation. In particular, $a_i=0$ implies that the field components E_ϕ and H_z vanish, and continuity of the remaining tangential field components E_z and H_ϕ at the boundary requires that

$$\begin{pmatrix} \frac{k_{1\perp}^2}{k_1^2} H_0(k_{1\perp}R) & -\frac{k_{2\perp}^2}{k_2^2} J_0(k_{2\perp}R) \\ \frac{i}{\omega\mu_0} k_{1\perp} H'_0(k_{1\perp}R) & -\frac{i}{\omega\mu_0} k_{2\perp} J'_0(k_{2\perp}R) \end{pmatrix} \begin{pmatrix} b_1 \\ b_2 \end{pmatrix} = \begin{pmatrix} 0 \\ 0 \end{pmatrix}. \tag{A5}$$

Setting the determinant of the above matrix equal to zero immediately yields the mode equation of Eq. (2), and it is also immediately seen that the ratio of the coefficients $b_{1,2}$ must be given by Eq. (4).

APPENDIX B: DERIVATION OF CUTOFF FOR HIGHER-ORDER MODES

In this section, we show that, to a very good approximation, a nanowire essentially supports a single, fundamental $m=0$ plasmon mode. In particular, for all higher-order plasmon modes $|m|\geq 2$, a cutoff wire size R_{cutoff} exists below which such modes cannot exist, while the $|m|=1$ plasmon modes exhibit an exponential growth in their mode volumes as $R\to 0$. For simplicity, we will assume in this section that we are dealing with a lossless system (Im $\epsilon_2=0$).

1. Behavior of $|m|\geq 2$ modes

We are interested here in the behavior of the $|m|\geq 2$ modes near cutoff, which is characterized by a small deviation of the plasmon wave vector $k_\parallel$ from $\sqrt{\epsilon_1}\omega/c$ (see Fig. 2). To simplify algebra in the derivation of R_{cutoff}, from this point forward we make the mode Eq. (1) dimensionless by setting $\omega/c=1$, and we will assume that m is positive (the case where m is negative follows this derivation with a few minor modifications). Furthermore, it is useful to define a small quantity $\delta=k_\parallel-\sqrt{\epsilon_1}$, where we specifically consider the positive $k_\parallel$ solution. On physical grounds, any mode with positive $k_\parallel$ must satisfy $\delta\geq 0$, because if $k_\parallel<\sqrt{\epsilon_1}$, the fields outside the wire would be radiative in nature and implies that the system is continually radiating energy out to infinity without a source. It follows that any value of R where $\delta=0$ becomes a solution to Eq. (1) for some m then corresponds to a critical point in behavior, and specifically is a cutoff beyond which modes cease to exist for that given m. To find this $R=R_{\text{cutoff}}$, we expand the two sides of Eq. (1) in δ. Both sides have contributions to these expansions that are divergent at $\delta=0$ (terms that behave like δ^{-n}, where $n>0$), and we will show that, for $m\geq 2$, there exists one value of R that equates these two divergent contributions; i.e., $\delta=0$ satisfies the mode equation at this particular value $R=R_{\text{cutoff}}$.

It is straightforward to show that the divergent contribution to the expansion of the left-hand side (LHS) of Eq. (1) is given by

$$\text{LHS} = \frac{m^2}{4R^2\delta^2} - \frac{m^2(3\epsilon_1+\epsilon_2)}{4R^2\sqrt{\epsilon_1}(\epsilon_1-\epsilon_2)\delta} + \mathcal{O}(\delta^0). \tag{B1}$$

To expand the right-hand side, we first note that the quantity $(1/k_{2\perp})J'_m(k_{2\perp}R)/J_m(k_{2\perp}R)=(1/\sqrt{\epsilon_2-\epsilon_1})\tilde{J}_m(\sqrt{\epsilon_2-\epsilon_1}R)+\mathcal{O}(\delta^1)$ is well behaved near $\delta=0$. Here, we have defined $\tilde{J}_m(x)=J'_m(x)/J_m(x)$. Then, using the identity

$$H_m(ix) = \frac{2}{\pi i^{m+1}} K_m(x), \tag{B2}$$

where $K_m(x)$ is a modified Bessel function of the second kind, and the expansions

$$K_m(x) = \frac{(m-1)!}{2}\left(\frac{2}{x}\right)^m - \frac{(m-2)!}{2}\left(\frac{2}{x}\right)^{m-2} + O(x^{4-m}) \quad (m\geq 2), \tag{B3}$$

$$k_{1\perp} = i\left[\sqrt{2\delta\sqrt{\epsilon_1}} + \frac{\delta^{3/2}}{2^{3/2}\epsilon_1^{1/4}} + \mathcal{O}(\delta^{5/2})\right] \tag{B4a}$$

$$\equiv i\kappa_{1\perp}, \tag{B4b}$$

it is tedious but straightforward to expand the expression $(1/k_{1\perp})[H'_m(k_{1\perp}R)/H_m(k_{1\perp}R)]$ as well. Performing these expansions and simplifying, one finds that

$$\mathrm{RHS} = \frac{m^2}{4R^2\delta^2} - \frac{m^2}{4R^2\sqrt{\epsilon_1}\delta} + \frac{m\sqrt{\epsilon_1}}{2(m-1)\delta} + \frac{im(\epsilon_1+\epsilon_2)\tilde{J}_m(\sqrt{\epsilon_2-\epsilon_1}R)}{2R\sqrt{\epsilon_1(\epsilon_1-\epsilon_2)}\delta} + \mathcal{O}(\delta^0). \quad \text{(B5)}$$

Comparing Eqs. (B1) and (B5), we see that $\delta=0$ is a solution provided that these terms are equal to $\mathcal{O}(\delta^{-1})$, i.e.,

$$\frac{m}{R}\frac{\epsilon_1+\epsilon_2}{\epsilon_2-\epsilon_1} = \frac{R\epsilon_1}{m-1} + \frac{i(\epsilon_1+\epsilon_2)\tilde{J}_m(\sqrt{\epsilon_2-\epsilon_1}R)}{\sqrt{\epsilon_1-\epsilon_2}}. \quad \text{(B6)}$$

The solution $R=R_{\mathrm{cutoff}}$ to Eq. (B6) gives the cutoff wire size, below which the mode m cannot exist. In the regime of interest ($\epsilon_1>0$, $\epsilon_2<0$, $\epsilon_1+\epsilon_2<0$), the first and second terms are positive while the third term is a negative function (for $R>0$) that behaves like $-1/R$ for small R and approaches a constant for large R. It can be seen then that a solution exists for any $m\geqslant 2$, which establishes that these modes are indeed cut off in the nanowire limit.

2. Behavior of $|m|=1$ mode

For simplicity, we will assume that $m=1$, as the case of $m=-1$ follows this derivation closely. The case of $m=1$ must be studied separately because the expansion of $K_m(x)$ given in Eq. (B3) only holds for $m\geqslant 2$. The different asymptotic scaling of $K_1(x)$ leads to a unique behavior of the $m=1$ mode in the nanowire limit. In particular, we will show that this mode does not strictly have a cutoff size, but that $k_\parallel \to \sqrt{\epsilon_1}$ exponentially in the limit $R\to 0$. In turn, the magnitude of $k_{1\perp}$ becomes exponentially small, which corresponds to an exponential growth in the spatial extent or mode volume.

Again defining $\delta=k_\parallel-\sqrt{\epsilon_1}$, we are interested in finding an approximate solution to Eq. (1) in the limit of small δ. We proceed by expanding both sides of the equation as a series in the small parameter. The expression for the left-hand side given by Eq. (B1) remains valid for $m=1$. For the right-hand side, we anticipate that both the quantities $k_{1\perp}R$ and $k_{1\perp}$ will be small as $R\to 0$ (these assumptions can be checked for consistency at the end of the calculation), and we thus expand around $k_{1\perp}R=0$ the term

$$\frac{1}{k_{1\perp}}\frac{H_1'(k_{1\perp}R)}{H_1(k_{1\perp}R)} = \frac{1}{i\kappa_{1\perp}}\frac{H_1'(i\kappa_{1\perp}R)}{H_1(i\kappa_{1\perp}R)} \quad \text{(B7a)}$$

$$= \frac{1}{i\kappa_{1\perp}}\left[\frac{i}{\kappa_{1\perp}R} - i\left(\gamma + \log\frac{\kappa_{1\perp}R}{2}\right)\kappa_{1\perp}R + O(\kappa_{1\perp}^2R^2)\right], \quad \text{(B7b)}$$

where $\gamma\approx 0.577$ is Euler's constant. Here, we have used Eq. (B2) to convert $H_m(ix)$ to $K_m(x)$ and the expansion

$$K_1(x) = \frac{1}{x} + \left(\frac{\gamma}{2} - \frac{\log 2}{2} - \frac{1}{4} + \frac{\log x}{2}\right)x + O(x^3). \quad \text{(B8)}$$

We now assume that $\kappa_{1\perp}R$ is small enough that $\gamma \ll |\log \kappa_{1\perp}R|$, such that

$$\frac{1}{k_{1\perp}}\frac{H_1'(k_{1\perp}R)}{H_1(k_{1\perp}R)} \approx \frac{1}{i\kappa_{1\perp}}\left(\frac{i}{\kappa_{1\perp}R} - i\kappa_{1\perp}R\log\frac{\kappa_{1\perp}R}{2}\right). \quad \text{(B9)}$$

Furthermore, having assumed that $k_{1\perp}$ (and by extension, $\kappa_{1\perp}$) is a small quantity, we can now expand the expression above in terms of δ using Eqs. (B4a) and (B4b). Making this substitution, and after a bit of algebra, one finds that the expansion of the right-hand side (RHS) of Eq. (1) is given by

$$\mathrm{RHS} \approx \frac{1}{4R^2\delta^2} + \frac{\epsilon_1+3\epsilon_2-2R^2\epsilon_1(\epsilon_1-\epsilon_2)\log(\delta R^2\sqrt{\epsilon_1}/2)}{4R^2\sqrt{\epsilon_1}(\epsilon_1-\epsilon_2)\delta}. \quad \text{(B10)}$$

Finally, equating the left- and right-hand sides to $\mathcal{O}(\delta^{-1})$ gives the solution

$$\delta \approx \frac{2}{R^2\sqrt{\epsilon_1}}\exp\left[-\frac{2(\epsilon_1+\epsilon_2)}{R^2\epsilon_1(\epsilon_2-\epsilon_1)}\right]. \quad \text{(B11)}$$

It follows that in the nanowire limit,

$$\kappa_{1\perp} = (k_\parallel^2-\epsilon_1)^{1/2} \quad \text{(B12a)}$$

$$\approx (2\delta\sqrt{\epsilon_1})^{1/2} \quad \text{(B12b)}$$

$$\approx \frac{2}{R}\exp\left[-\frac{\epsilon_1+\epsilon_2}{R^2\epsilon_1(\epsilon_2-\epsilon_1)}\right]. \quad \text{(B12c)}$$

Equations (B11) and (B12c) indicate that the $m=1$ plasmon mode does not have a cutoff in the nanowire limit, but instead that its longitudinal wave vector approaches $\sqrt{\epsilon_1}$ exponentially, with a corresponding exponential increase in its transverse extent ($\sim 1/\kappa_{1\perp}$) and mode volume. It is therefore well justified to say that this mode is effectively cut off, as the coupling strength to this mode becomes strongly suppressed as $R\to 0$.

APPENDIX C: RADIATIVE AND NONRADIATIVE DECAY RATES NEAR A NANOTIP

Here, we derive more carefully the expressions given in Eqs. (41) and (42) for the radiative and nonradiative spontaneous emission rates near a nanotip.

To calculate the radiative rate, we consider our expression for Φ_r in Eq. (36) in the far-field (large v) limit, where the $K_m(qv)$ terms in Φ_r decay exponentially with v. Because of this exponential dependence at large v, to good approximation, it suffices to expand the terms $\alpha_m(q)$, $J_m(qu')$, and $K_m(qv')$ around $q=0$. The only nontrivial expansions occur for the terms $\alpha_m(q)$ and are given by

$$\alpha_0(q) = \frac{1}{2}\left(1-\frac{\epsilon_2}{\epsilon_1}\right)q^2v_0^2 + \mathcal{O}(q^4), \quad \text{(C1)}$$

$$\alpha_1(q) = \frac{1}{2}\frac{\epsilon_1-\epsilon_2}{\epsilon_1+\epsilon_2}q^2v_0^2 + \mathcal{O}(q^4), \quad \text{(C2)}$$

and so on. These expansions allow for exact evaluations of the integral. It can be verified that the dipole contributions to

Φ_r originate from the $m=0,1$ terms in the sum, which are readily found to be

$$\Phi_r^{(m=0)}(\mathbf{r},\mathbf{r}') \approx \frac{1}{4\pi\epsilon_0\epsilon_1} v_0^2 \left(1-\frac{\epsilon_2}{\epsilon_1}\right) \frac{4(v^2-u^2)}{(u^2+v^2)^3} \ln\frac{v}{v'} + \delta\Phi(\mathbf{r}), \tag{C3}$$

$$\Phi_r^{(m=1)}(\mathbf{r},\mathbf{r}') \approx \frac{1}{4\pi\epsilon_0\epsilon_1} \cos(\phi-\phi') \frac{\epsilon_1-\epsilon_2}{\epsilon_1+\epsilon_2} \frac{v_0^2 u'}{v'} \frac{8uv}{(u^2+v^2)^3}. \tag{C4}$$

Here, $\delta\Phi$ is a complicated function, but, most importantly, contains no dependence on $\mathbf{r}'$. Recalling that the pseudopotentials derived above correspond to a point charge source, we can immediately obtain the potentials due to a dipole $\mathbf{p_0}e^{-i\omega t}$ at $\mathbf{r}'$ by applying the operator $(\mathbf{p_0}\cdot\nabla')$ to these expressions. In parabolic coordinates, the gradient operator is given by

$$\nabla = \frac{1}{\sqrt{u^2+v^2}}\left(\hat{u}\frac{\partial}{\partial u} + \hat{v}\frac{\partial}{\partial v}\right) + \frac{1}{uv}\hat{\phi}\frac{\partial}{\partial\phi}, \tag{C5}$$

and for a dipole located on the z axis ($u'=0$), we find that

$$\Phi_{dip,r}^{(m=0)} \approx -\frac{1}{4\pi\epsilon_0\epsilon_1}\left(1-\frac{\epsilon_2}{\epsilon_1}\right)\frac{v_0^2}{v'^2}\frac{(\hat{v}\cdot\mathbf{r})(\mathbf{p_0}\cdot\hat{v})}{r^3}, \tag{C6}$$

$$\Phi_{dip,r}^{(m=1)} \approx \frac{1}{4\pi\epsilon_0\epsilon_1}\frac{\epsilon_1-\epsilon_2}{\epsilon_1+\epsilon_2}\frac{v_0^2}{v'^2}\frac{[\mathbf{p_0}-\hat{v}(\mathbf{p_0}\cdot\hat{v})]\cdot\mathbf{r}}{r^3}. \tag{C7}$$

From these expressions, one can immediately identify the induced dipole moments in the nanotip,

$$\delta\mathbf{p} = -\hat{v}p_0\frac{v_0^2}{v'^2}\left(1-\frac{\epsilon_2}{\epsilon_1}\right) \quad (\mathbf{p_0}\parallel\hat{z}), \tag{C8}$$

$$\delta\mathbf{p} = \hat{u}p_0\frac{\epsilon_1-\epsilon_2}{\epsilon_1+\epsilon_2}\frac{v_0^2}{v'^2} \quad (\mathbf{p_0}\perp\hat{z}), \tag{C9}$$

and arrive at the radiative decay rates given in Eq. (41).

The leading term for the nonradiative decay rate is found by calculating the divergence in the reflected field $\mathbf{E}_r(\mathbf{r}',\mathbf{r}')$ as $v'\to v_0$. The reflected field $\mathbf{E}_r=-\nabla(\mathbf{p_0}\cdot\nabla')\Phi_r$ is, in general, difficult to evaluate, but simplifies considerably for a dipole located on-axis ($u'=0$) due to the presence of the $J_m(qu')$ term in Φ_r, given in Eq. (36). The operation ∇' causes terms like $J_m(0)$ and $J_m'(0)$ to appear in $\mathbf{E}_r$, which are nonzero only when $m=0$ and $m=1$, respectively. This immediately leads to the expressions

$$\mathbf{p_0}\cdot\mathbf{E}_r(\mathbf{r}',\mathbf{r}') = -\frac{p_0^2}{4\pi\epsilon_0\epsilon_1}\int_0^\infty dq\frac{q^3}{v'^2}\alpha_1(q)K_1^2(qv') \quad (\mathbf{p_0}\perp\hat{z}),$$

$$\mathbf{p_0}\cdot\mathbf{E}_r(\mathbf{r}',\mathbf{r}') = -\frac{p_0^2}{2\pi\epsilon_0\epsilon_1}\int_0^\infty dq\frac{q^3}{v'^2}\alpha_0(q)K_1^2(qv') \quad (\mathbf{p_0}\parallel\hat{z}), \tag{C10}$$

which were given in Eq. (40). Examining further the solutions to $\alpha_{0,1}$, it can easily be shown that their asymptotic expansions in the limit $qv_0\gg 1$ take the form

$$\alpha_{0,1}(q) \approx \frac{1}{\pi}\frac{\epsilon_1-\epsilon_2}{\epsilon_1+\epsilon_2}e^{2qv_0} \quad (qv_0\gg 1). \tag{C11}$$

At the same time, in the limit $qv'\gg 1$, the behavior of K_1^2 is given by $K_1^2(qv')\approx(\pi/2qv')e^{-2qv'}$, and thus, as $v'\to v_0$ the integrands of Eq. (C10) exhibit very long tails due to the presence of terms $\sim e^{-2q(v'-v_0)}$ at large q. The tail is the origin of the divergence that we expect on physical grounds. Using these expansions as well as the fact that the decay rate is proportional to $\mathrm{Im}(\mathbf{p_0}\cdot\mathbf{E})$, the integrals can be evaluated exactly and yield the nonradiative decay rates given in Eq. (42).

APPENDIX D: BOUNDARY ELEMENT METHOD

Our numerical implementation of the boundary element method (BEM) closely follows the method derived in Ref. 40. Here, we briefly outline the main ideas of BEM while referring the reader to Ref. 40 for more details, and we discuss the key elements of our implementation.

We assume that our system contains a set of known, time-harmonic source charges and currents $\rho_{\mathrm{ext}},\mathbf{j}_{\mathrm{ext}}$ in the presence of some scattering dielectric body whose surface is denoted S (although we discuss one body here, BEM is easily generalizable to treat multiple scatterers). In the case of interest, S represents the surface of a metallic nanotip, while the external source corresponds to an oscillating point dipole $\mathbf{p_0}e^{-i\omega t}$ at some location $\mathbf{r}'$. For simplicity, we also assume that we are working with nonmagnetic media, and we denote by ϵ_j ($j=1,2$) the dimensionless electric permittivities outside and inside S, respectively. The underlying principle behind BEM is that the scalar and vector potentials $\phi_j(\mathbf{r})$ and $\mathbf{A}_j(\mathbf{r})$ in each region can be written (in the Lorentz gauge) in the form

$$\phi_j(\mathbf{r}) = \frac{1}{4\pi\epsilon_0\epsilon_j}\int d\mathbf{r}' G_j(\mathbf{r}-\mathbf{r}')\rho_{\mathrm{ext}}(\mathbf{r}') + \frac{1}{4\pi\epsilon_0\epsilon_j}\int_S d\mathbf{s} \times G_j(\mathbf{r}-\mathbf{s})\sigma_j(\mathbf{s}), \tag{D1}$$

$$\mathbf{A}_j(\mathbf{r}) = \frac{\mu_0}{4\pi}\int d\mathbf{r}' G_j(\mathbf{r}-\mathbf{r}')\mathbf{j}_{\mathrm{ext}}(\mathbf{r}') + \frac{\mu_0}{4\pi}\int_S d\mathbf{s} G_j(\mathbf{r}-\mathbf{s})\mathbf{h}_j(\mathbf{s}), \tag{D2}$$

$$G_j(\mathbf{r}) = \frac{e^{ik_j r}}{r}, \tag{D3}$$

where G_j is the Green's function in a medium of uniform ϵ_j, and $k_j=\sqrt{\epsilon_j}(\omega/c)$. Physically, the equations above state that the fields in region j can be described as a result of the combination of the external sources and some effective surface charge and current distributions σ_j and $\mathbf{h}_j$ on S. In general, these effective distributions do not have physical significance; for example, they do not correspond to actual charges and currents, and the distributions in region 1 and region 2 are not necessarily equal [e.g., $\sigma_1(\mathbf{s})\neq\sigma_2(\mathbf{s})$]. The

values of σ_j and $\mathbf{h}_j$ are not known initially, but a set of linear integral equations for these distributions results from enforcing various boundary conditions for the scalar and vector potentials at S. In particular, ϕ, $\mathbf{A}$, $\mathbf{D}_\perp$, and $\mathbf{H}_\parallel$ must be continuous at the boundary. To calculate the distributions numerically, if the boundary S is finite, one can mesh up the surface into a finite number of grid points. Assuming that σ_j and $\mathbf{h}_j$ are constant over each grid point, the linear integral equations become a set of linear equations in the values of σ_j and $\mathbf{h}_j$ that can be solved straightforwardly. Once these distributions are known, the potentials and then the fields $\mathbf{E}$ and $\mathbf{H}$ can be calculated.

In our problem of interest, we assume that the dipole is located on the z axis and oriented along $\hat{z}$, while the nanotip is described by a paraboloid of revolution around the z axis. Due to the axial symmetry of the system, BEM simulations are advantageous because one only needs to calculate the unknown distributions along one dimension instead of over the entire two-dimensional surface S. At the same time, the source is a dipole oscillating at constant frequency, and thus, the external charges and currents are calculated quite easily. In BEM (at least in the current formulation), it is necessary that the nanotip surface S be finite, and we implement this numerically by tapering and rounding off the nanotip far from the region of interest. In general, any termination can result in some back reflection of the guided plasmon, and this results in some small oscillations of the fields due to interference with the forward propagating plasmon, as barely seen, e.g, in Fig. 5. In our simulations, the reflected amplitude is kept to within a few percent. Very fine meshes were used to ensure accuracy; in most of our simulations, for example, the spacing between points in the regions of constant R was approximately $\lambda_{\mathrm{pl}}/400$.

APPENDIX E: DERIVATION OF COUPLED-MODE EQUATIONS

In this section, we derive the equations of evolution for two electromagnetically coupled systems based on Lorentz reciprocity.

First, we derive the Lorentz reciprocity equation generally. Assuming nonmagnetic media, suppose that $\{\mathbf{E}_1(\mathbf{r}),\mathbf{H}_1(\mathbf{r}),\epsilon_1(\mathbf{r})\}$ and $\{\mathbf{E}_2(\mathbf{r}),\mathbf{H}_2(\mathbf{r}),\epsilon_2(\mathbf{r})\}$ separately satisfy Maxwell's equations. At this point, the systems 1 and 2 and their field solutions are not necessarily related to each other at all. In the following, we assume that all fields $\mathbf{E}(\mathbf{r},t)=\mathbf{E}(\mathbf{r})e^{-i\omega t}$,$\mathbf{H}(\mathbf{r},t)=\mathbf{H}(\mathbf{r})e^{-i\omega t}$ have harmonic time dependence. Using the vector identity

$$\nabla\cdot(\mathbf{a}\times\mathbf{b})=\mathbf{b}\cdot(\nabla\times\mathbf{a})-\mathbf{a}\cdot(\nabla\times\mathbf{b}) \tag{E1}$$

and the curl relations of Maxwell's equations, we can write

$$\begin{aligned}\nabla\cdot(\mathbf{E}_1\times\mathbf{H}_2^*)&=\mathbf{H}_2^*\cdot(\nabla\times\mathbf{E}_1)-\mathbf{E}_1\cdot(\nabla\times\mathbf{H}_2^*)\\&=\mathbf{H}_2^*\cdot(i\omega\mu_0\mathbf{H}_1)-\mathbf{E}_1\cdot(i\omega\epsilon_0\epsilon_2^*\mathbf{E}_2^*),\end{aligned} \tag{E2}$$

and similarly,

$$\begin{aligned}\nabla\cdot(\mathbf{E}_2^*\times\mathbf{H}_1)&=\mathbf{H}_1\cdot(\nabla\times\mathbf{E}_2^*)-\mathbf{E}_2^*\cdot(\nabla\times\mathbf{H}_1)\\&=\mathbf{H}_1\cdot(-i\omega\mu_0\mathbf{H}_2^*)-\mathbf{E}_2^*\cdot(-i\omega\epsilon_0\epsilon_1\mathbf{E}_1).\end{aligned} \tag{E3}$$

Adding up Eqs. (E2) and (E3) yields the equation for Lorentz reciprocity,

$$\nabla\cdot(\mathbf{E}_1\times\mathbf{H}_2^*+\mathbf{E}_2^*\times\mathbf{H}_1)=i\omega\epsilon_0\mathbf{E}_1\cdot\mathbf{E}_2^*[\epsilon_1(\mathbf{r})-\epsilon_2^*(\mathbf{r})]. \tag{E4}$$

We now derive coupled-mode equations for two waveguides based on the Lorentz reciprocity equation above. This derivation closely follows that of Ref. 46. We emphasize that the nature of the waveguides can be quite general; e.g., they can be any type of normal dielectric or plasmon waveguide. We let the indices $\mu,\nu=a,b$ refer to the system consisting of waveguide a without the presence of system b, and b the system consisting of waveguide b without the presence of a. We also assume that the surrounding dielectrics for systems a and b are the same, i.e., $\epsilon_a(r=\infty)=\epsilon_b(r=\infty)$, and that the waveguides are copropagating along the z direction. It is assumed that the total electric field for the system consisting of waveguides a and b together can be written as

$$\mathbf{E}_T(\mathbf{r})=\sum_{\nu=a,b}C_\nu(z)\mathbf{E}_\nu(\mathbf{r}), \tag{E5}$$

with a similar expression for $\mathbf{H}$. That is, we assume that the total field can be written as a linear superposition of the unperturbed modes of systems a and b. For the case where systems a and b each have one allowed mode, the index ν refers to these unperturbed modes. In general, when a and b have $N_{a,b}$ allowed unperturbed modes, ν is understood to be an index that covers all of these modes. We can derive exact equations of motion for $C_\nu(z)$ by using Eq. (E4). Specifically, we will let the index $1=T$ in Eq. (E4) refer to the total fields $\mathbf{E}_T(\mathbf{r})$ and $\mathbf{H}_T(\mathbf{r})$ and the dielectric profile of the combined system $\epsilon_T(\mathbf{r})$, while we will let the index $2=\mu$ refer to any one of the allowed, unperturbed modes of systems a and b. Substituting this into Eq. (E4) yields

$$\nabla\cdot(\mathbf{E}_T\times\mathbf{H}_\mu^*+\mathbf{E}_\mu^*\times\mathbf{H}_T)=i\omega\epsilon_0\mathbf{E}_T\cdot\mathbf{E}_\mu^*[\epsilon_T(\mathbf{r})-\epsilon_\mu^*(\mathbf{r})] \tag{E6}$$

or

$$\begin{aligned}\sum_{\nu=a,b}\nabla\cdot[C_\nu(z)\mathbf{E}_\nu\times\mathbf{H}_\mu^*+C_\nu(z)\mathbf{E}_\mu^*\times\mathbf{H}_\nu]\\=i\omega\epsilon_0\sum_{\nu=a,b}C_\nu(z)\mathbf{E}_\nu\cdot\mathbf{E}_\mu^*[\epsilon_T(\mathbf{r})-\epsilon_\mu^*(\mathbf{r})].\end{aligned} \tag{E7}$$

Applying the divergence theorem to this result (and assuming that the surface terms vanish at infinity) gives

$$\begin{aligned}\frac{\partial}{\partial z}\sum_{\nu=a,b}\int d^2\boldsymbol{\rho}[C_\nu(z)\mathbf{E}_\nu\times\mathbf{H}_\mu^*+C_\nu(z)\mathbf{E}_\mu^*\times\mathbf{H}_\nu]\cdot\hat{z}\\=i\omega\epsilon_0\sum_{\nu=a,b}C_\nu(z)\int d^2\boldsymbol{\rho}\mathbf{E}_\nu\cdot\mathbf{E}_\mu^*[\epsilon_T(\mathbf{r})-\epsilon_\mu^*(\mathbf{r})].\end{aligned} \tag{E8}$$

The left-hand side can be further simplified,

$$\text{LHS} = \frac{\partial}{\partial z}\sum_{\nu=a,b}\int d^2\boldsymbol{\rho}[C_\nu(z)\mathbf{E}_\nu \times \mathbf{H}_\mu^* + C_\nu(z)\mathbf{E}_\mu^* \times \mathbf{H}_\nu]\cdot\hat{z} \tag{E9a}$$

$$= \sum_{\nu=a,b}\frac{dC_\nu}{dz}\left[\int d^2\boldsymbol{\rho}(\mathbf{E}_\nu \times \mathbf{H}_\mu^* + \mathbf{E}_\mu^* \times \mathbf{H}_\nu)\cdot\hat{z}\right] + C_\nu(z)\left[\frac{\partial}{\partial z}\int d^2\boldsymbol{\rho}(\mathbf{E}_\nu \times \mathbf{H}_\mu^* + \mathbf{E}_\mu^* \times \mathbf{H}_\nu)\cdot\hat{z}\right] \tag{E9b}$$

$$= \sum_{\nu=a,b}\frac{dC_\nu}{dz}\left[\int d^2\boldsymbol{\rho}(\mathbf{E}_\nu \times \mathbf{H}_\mu^* + \mathbf{E}_\mu^* \times \mathbf{H}_\nu)\cdot\hat{z}\right] + C_\nu(z)\left(i\omega\epsilon_0\int d^2\boldsymbol{\rho}\mathbf{E}_\nu\cdot\mathbf{E}_\mu^*[\boldsymbol{\epsilon}_\nu(\mathbf{r}) - \boldsymbol{\epsilon}_\mu^*(\mathbf{r})]\right), \tag{E9c}$$

where we have applied the divergence theorem on Eq. (E4) to get the last line.

Substituting Eq. (E9c) back into Eq. (E8) yields a set of N_a+N_b coupled, first-order differential equations:

$$\sum_\nu \frac{dC_\nu}{dz}P_{\nu\mu}(z) = -i\omega\epsilon_0\sum_\nu C_\nu(z)K_{\nu\mu}(z), \tag{E10}$$

$$P_{\nu\mu}(z) \equiv \int d^2\boldsymbol{\rho}(\mathbf{E}_\nu \times \mathbf{H}_\mu^* + \mathbf{E}_\mu^* \times \mathbf{H}_\nu)\cdot\hat{z}, \tag{E11}$$

$$K_{\nu\mu}(z) \equiv \int d^2\boldsymbol{\rho}\mathbf{E}_\nu\cdot\mathbf{E}_\mu^*[\boldsymbol{\epsilon}_\nu(\mathbf{r}) - \boldsymbol{\epsilon}_T(\mathbf{r})]. \tag{E12}$$

We emphasize that these coupled-mode equations are exact within the ansatz given by Eq. (E5).

APPENDIX F: RADIATIVE SCATTERING

Suppose that in the presence of roughness, the first-order scattered field E_z is given by Eq. (59). Using the expressions derived in Eq. (3) for the unperturbed, incident plasmon field, and letting $k_\parallel$ denote the unperturbed plasmon wave vector, the total (incident plus scattered) fields to first order in p are given by

$$\mathbf{E}_1^{\text{total}} = \left[\frac{ik_\parallel k_{1\perp}}{k_1^2}b_1H_0'(k_{1\perp}\rho)e^{ik_\parallel z} + p\int_{-\infty}^{\infty}dh_\parallel\frac{ih_\parallel h_{1\perp}}{k_1^2}H_0'(h_{1\perp}\rho)e^{ih_\parallel z}A(h_\parallel)\right]\hat{\rho} + \left[\frac{k_{1\perp}^2}{k_1^2}b_1H_0(k_{1\perp}\rho)e^{ik_\parallel z} + p\int_{-\infty}^{\infty}dh_\parallel\frac{h_{1\perp}^2}{k_1^2}H_0(h_{1\perp}\rho)e^{ih_\parallel z}A(h_\parallel)\right]\hat{z},$$

$$\mathbf{E}_2^{\text{total}} = \left[\frac{ik_\parallel k_{2\perp}}{k_2^2}b_2J_0'(k_{2\perp}\rho)e^{ik_\parallel z} + p\int_{-\infty}^{\infty}dh_\parallel\frac{ih_\parallel h_{2\perp}}{k_2^2}J_0'(h_{2\perp}\rho)e^{ih_\parallel z}B(h_\parallel)\right]\hat{\rho} + \left[\frac{k_{2\perp}^2}{k_2^2}b_2J_0(k_{2\perp}\rho)e^{ik_\parallel z} + p\int_{-\infty}^{\infty}dh_\parallel\frac{h_{2\perp}^2}{k_2^2}J_0(h_{2\perp}\rho)e^{ih_\parallel z}B(h_\parallel)\right]\hat{z},$$

$$H_{1,\phi}^{\text{total}} = \frac{1}{\omega\mu_0}\left[ik_{1\perp}b_1H_0'(k_{1\perp}\rho)e^{ik_\parallel z} + p\int_{-\infty}^{\infty}dh_\parallel ih_{1\perp}H_0'(h_{1\perp}\rho)e^{ih_\parallel z}A(h_\parallel)\right],$$

$$H_{2,\phi}^{\text{total}} = \frac{1}{\omega\mu_0}\left[ik_{2\perp}J_0'(k_{2\perp}\rho)b_2e^{ik_\parallel z} + p\int_{-\infty}^{\infty}dh_\parallel ih_{2\perp}J_0'(h_{2\perp}\rho)e^{ih_\parallel z}B(h_\parallel)\right]. \tag{F1}$$

The boundary condition equations in Eq. (60) can be solved by plugging in the fields above, carefully expanding the equations as a power series in p, and then solving for each order of p, utilizing the expansions

$$\hat{t} = \hat{z} + p\frac{d\zeta}{dz}\hat{\rho} + \mathcal{O}(p^2),$$

$$F_{i,m}(k_{i\perp}\rho_0) = F_{i,m}(k_{i\perp}R) + p\zeta k_{i\perp}F_{i,m}'(k_{i\perp}R) + \mathcal{O}(p^2),$$

$$F_{i,m}(h_{i\perp}\rho_0) = F_{i,m}(h_{i\perp}R) + p\zeta h_{i\perp}F_{i,m}'(h_{i\perp}R) + \mathcal{O}(p^2), \tag{F2}$$

where $F_{1,m}(x)=H_m(x)$ and $F_{2,m}(x)=J_m(x)$. The resulting $\mathcal{O}(p^0)$ equations are trivially satisfied by the plasmon fields of a smooth nanowire, while the $\mathcal{O}(p)$ equations are found to be

$$\int_{-\infty}^{\infty}dh_\parallel\left[\frac{h_{1\perp}^2}{k_1^2}H_0(h_{1\perp}R)A(h_\parallel) - \frac{h_{2\perp}^2}{k_2^2}J_0(h_{2\perp}R)B(h_\parallel)\right]e^{ih_\parallel z} = \left[\frac{k_{2\perp}^3}{k_2^2}b_2\zeta(z)J_0'(k_{2\perp}R) - \frac{k_{1\perp}^3}{k_1^2}b_1\zeta(z)H_0'(k_{1\perp}R) + \frac{ik_\parallel k_{2\perp}}{k_2^2}b_2\frac{d\zeta}{dz}J_0'(k_{2\perp}R) - \frac{ik_\parallel k_{1\perp}}{k_1^2}b_1\frac{d\zeta}{dz}H_0'(k_{1\perp}R)\right]e^{ik_\parallel z},$$

$$\int_{-\infty}^{\infty}dh_\parallel[h_{1\perp}H_0'(h_{1\perp}R)A(h_\parallel) - h_{2\perp}J_0'(h_{2\perp}R)B(h_\parallel)]e^{ih_\parallel z} = [k_{2\perp}^2b_2\zeta(z)J_0''(k_{2\perp}R) - k_{1\perp}^2b_1\zeta(z)H_0''(k_{1\perp}R)]e^{ik_\parallel z}. \tag{F3}$$

Here, we assume that the metal inherently has no losses, i.e.,

Im $\epsilon_2=0$, such that $k_\parallel$ is purely real. Then, by plugging in the Fourier transform of $\zeta(z)$ given in Eq. (61), the equations above become purely algebraic. It is tedious but straightforward to show that the solutions are given by Eq. (62), with the coefficients $f(h_\parallel)$ and $g(h_\parallel)$ defined via

$$f(h_\parallel) = \frac{h_{2\perp} N J_0(h_{2\perp}R) - k_2^2 M(h_\parallel) J_0'(h_{2\perp}R)}{H_0(h_{1\perp}R) J_0' 2 \perp h_{1\perp} k_2^2 - H_0'(h_{1\perp}R) J_0(h_{2\perp}R) h_{2\perp} k_1^2},$$

$$g(h_\parallel) = \frac{h_{1\perp} N H_0(h_{1\perp}R) - k_1^2 M(h_\parallel) H_0'(h_{1\perp}R)}{H_0(h_{1\perp}R) J_0' 2 \perp h_{1\perp} k_2^2 - H_0'(h_{1\perp}R) J_0(h_{2\perp}R) h_{2\perp} k_1^2},$$

$$M(h_\parallel) = \left[\frac{k_{1\perp}^3}{k_1^2} - \frac{k_\parallel k_{1\perp}(h_\parallel - k_\parallel)}{k_1^2} \right] b_1 H_0'(k_{1\perp}R) - \left[\frac{k_{2\perp}^3}{k_2^2} - \frac{k_\parallel k_{2\perp}(h_\parallel - k_\parallel)}{k_2^2} \right] b_2 J_0'(k_{2\perp}R),$$

$$N = b_1 k_{1\perp}^2 H_0''(k_{1\perp}R) - b_2 k_{2\perp}^2 J_0''(k_{2\perp}R). \tag{F4}$$

To evaluate the expression for $\Gamma_{\mathrm{rad,rough}}$ in Eq. (68), we first normalize the fields such that the denominator takes the value $\hbar\omega/4L$. For concreteness, we assume that the conducting nanowire exhibits a Drude-like behavior and that we are operating well below the plasma frequency, such that $\epsilon_2(\omega) = 1 - \omega_p^2/\omega^2 \approx -\omega_p^2/\omega^2$. In this case, the dispersive term in the denominator is positive and given by $\frac{d}{d\omega}[\omega\epsilon_2(\omega)] \approx |\epsilon_2(\omega)|$. In the nanowire limit, normalization of the integral is straightforward and yields a coefficient $b_1 \approx \sqrt{\hbar\omega k_0^4 \epsilon_1^2 R^2/\epsilon_0 \tilde{V} \tilde{C}^4 L}$. Here, $\tilde{V}$ is a dimensionless parameter given by

$$\tilde{V} = \frac{8\epsilon_1^2}{\pi C^2} \left(\frac{K_1^2(C)}{|\epsilon_2| I_1^2(C)} \int_0^C dx x [I_1^2(x) + I_0^2(x)] + \frac{1}{\epsilon_1} \int_C^\infty dx x [K_1^2(x) + K_0^2(x)] \right). \tag{F5}$$

Then, using the relationships $k_\parallel \approx C/R$ and $k_{i\perp} \approx iC/R$, one can calculate the leading terms of $f(h_\parallel)$ as $R \to 0$,

$$f(h_\parallel) \approx \frac{h_{2\perp} b_1 (C/R)^2 \phi}{-2ik_1^2 h_{2\perp}/\pi h_{1\perp} R}, \tag{F6}$$

where we have defined $\phi \equiv (b_2/b_1) J_0''(iC) - H_0''(iC)$. In the equation above, we have explicitly given the leading terms of the numerator and denominator of $f(h_\parallel)$. The ratio b_1/b_2 is given in Eq. (4), which in the nanowire limit results in the simplification of ϕ given in Eq. (70).

APPENDIX G: NONRADIATIVE SCATTERING

The elements of the matrices M_i and vectors $\mathbf{v}_i$ appearing in the matrix integral Eq. (79) in the presence of surface roughness are given by

$$M_0(h) = \begin{pmatrix} \tilde{K}_m(hR) & -\tilde{I}_m(hR) \\ h\epsilon_1 \tilde{K}_m'(hR) & -h\epsilon_2 \tilde{I}_m'(hR) \end{pmatrix}, \tag{G1}$$

$$M_1(h,q) = \begin{pmatrix} q\tilde{K}_m'(qR) & -q\tilde{I}_m'(qR) \\ \epsilon_1[q^2\tilde{K}_m''(qR) + q(h-q)\tilde{K}_m(qR)] & -\epsilon_2[q^2\tilde{I}_m''(qR) + q(h-q)\tilde{I}_m(qR)] \end{pmatrix} e^{i(h-q)z'}, \tag{G2}$$

$$M_2(h,q,q') = \begin{pmatrix} \frac{q^2}{2}\tilde{K}_m''(qR) & -\frac{q^2}{2}\tilde{I}_m''(qR) \\ M_2^{21}(h,q,q') & M_2^{22}(h,q,q') \end{pmatrix} e^{i(h-q)z'}, \tag{G3}$$

$$M_2^{21}(h,q,q') = \epsilon_1 \left[\frac{q^3}{2}\tilde{K}_m'''(qR) + q^2(h-q-q')\tilde{K}_m'(qR) + \frac{1}{2}qq'(h-q-q')\tilde{K}_m'(qR) \right], \tag{G4}$$

$$M_2^{22}(h,q,q') = -\epsilon_2 \left[\frac{q^3}{2}\tilde{I}_m'''(qR) + q^2(h-q-q')\tilde{I}_m'(qR) + \frac{1}{2}qq'(h-q-q')\tilde{I}_m'(qR) \right], \tag{G5}$$

$$\mathbf{v}_0(h) = -\begin{pmatrix} \tilde{I}_m(hR) \\ h\tilde{I}_m'(hR) \end{pmatrix} \tilde{K}_m(h\rho'), \tag{G6}$$

$$\mathbf{v}_1(h,q) = -\begin{pmatrix} q\tilde{I}_m'(qR) \\ q^2\tilde{I}_m''(qR) + q(h-q)\tilde{I}_m(qR) \end{pmatrix} \tilde{K}_m(q\rho') e^{i(h-q)z'}, \tag{G7}$$

$$\mathbf{v}_2(h,q,q') = -\begin{pmatrix} \frac{q^2}{2}\tilde{I}''_m(qR) \\ \frac{q^3}{2}\tilde{I}'''_m(qR) + q^2(h-q-q')\tilde{I}'_m(qR) + \frac{1}{2}qq'(h-q-q')\tilde{I}'_m(qR) \end{pmatrix} \tilde{K}_m(q\rho')e^{i(h-q)z'}. \quad \text{(G8)}$$

[1] For a review, see, e. g., A. V. Zayats and I. I. Smolyaninov, J. Opt. A, Pure Appl. Opt. **5**, S16 (2003).
[2] K. Kneipp, Y. Wang, H. Kneipp, L. T. Perelman, I. Itzkan, R. R. Dasari, and M. S. Feld, Phys. Rev. Lett. **78**, 1667 (1997).
[3] S. Nie and S. R. Emory, Science **275**, 1102 (1997).
[4] T. W. Ebbesen *et al.*, Nature (London) **391**, 667 (1998).
[5] T. Thio *et al.*, Opt. Lett. **26**, 1972 (2001).
[6] N. E. Hecker *et al.*, Appl. Phys. Lett. **75**, 1577 (1999).
[7] S. J. Oldenburg *et al.*, Anal. Biochem. **309**, 109 (2002).
[8] I. I. Smolyaninov, J. Elliott, A. V. Zayats, and C. C. Davis, Phys. Rev. Lett. **94**, 057401 (2005).
[9] A. V. Zayats *et al.*, Appl. Phys. Lett. **86**, 151114 (2005).
[10] J. Takahara *et al.*, Opt. Lett. **22**, 475 (1997).
[11] M. Quinten *et al.*, Opt. Lett. **23**, 1331 (1998).
[12] M. L. Brongersma, J. W. Hartman, and H. A. Atwater, Phys. Rev. B **62**, R16356 (2000).
[13] S. I. Bozhevolnyi *et al.*, Nature (London) **440**, 508 (2006).
[14] R. M. Dickson and L. A. Lyon, J. Phys. Chem. B **104**, 6095 (2000).
[15] J. R. Krenn *et al.*, Europhys. Lett. **60**, 663 (2002).
[16] H. Ditlbacher, A. Hohenau, D. Wagner, U. Kreibig, M. Rogers, F. Hofer, F. R. Aussenegg, and J. R. Krenn, Phys. Rev. Lett. **95**, 257403 (2005).
[17] A. K. Ekert, Phys. Rev. Lett. **67**, 661 (1991).
[18] H.-J. Briegel, W. Dur, J. I. Cirac, and P. Zoller, Phys. Rev. Lett. **81**, 5932 (1998).
[19] K. M. Svore, B. M. Terhal, and D. P. DiVincenzo, Phys. Rev. A **72**, 022317 (2005).
[20] R. J. Thompson, G. Rempe, and H. J. Kimble, Phys. Rev. Lett. **68**, 1132 (1992).
[21] M. Brune, F. Schmidt-Kaler, A. Maali, J. Dreyer, E. Hagley, J. M. Raimond, and S. Haroche, Phys. Rev. Lett. **76**, 1800 (1996).
[22] A. Wallraff *et al.*, Nature (London) **431**, 162 (2004).
[23] L. Childress, A. S. Sørensen, and M. D. Lukin, Phys. Rev. A **69**, 042302 (2004).
[24] A. S. Sørensen, C. H. van der Wal, L. I. Childress, and M. D. Lukin, Phys. Rev. Lett. **92**, 063601 (2004).
[25] A. Blais, R. S. Huang, A. Wallraff, S. M. Girvin, and R. J. Schoellkopf, Phys. Rev. A **69**, 062320 (2004).
[26] J. A. Stratton, *Electromagnetic theory*, 1st ed. (McGraw-Hill, New York, 1941), Chap. 9.
[27] J. D. Jackson, *Classical Electrodynamics*, 3rd ed. (Wiley, New York, 1999).
[28] P. B. Johnson and R. W. Christy, Phys. Rev. B **6**, 4370 (1972).
[29] We also note that there is some disagreement in the imaginary part of the electric permittivity at this frequency. Other meaurements, for example, indicate that the imaginary part may be a factor of ~4 higher than the value used here. See, e. g., M. A. Ordal *et al.*, Appl. Opt. **22**, 1099 (1983).
[30] L. Tong, J. Lou, and E. Mazur, Opt. Express **12**, 1025 (2004).
[31] J. A. McKay and J. A. Rayne, Phys. Rev. B **13**, 673 (1976).
[32] The use of these modes in the terahertz domain has also been explored recently in, e.g., Q. Cao and J. Jahns, Opt. Express **13**, 522 (2005).
[33] E. M. Purcell, Phys. Rev. **69**, 681 (1946).
[34] V. V. Klimov and M. Ducloy, Phys. Rev. A **69**, 013812 (2004).
[35] See, e.g., J. M. Wylie and J. E. Sipe, Phys. Rev. A **30**, 1185 (1984).
[36] Here, we take the spontaneous emission rate in uniform dielectric ϵ_1 to be $\Gamma_0 = \sqrt{\epsilon_1}\Gamma_v$, where Γ_v is the vacuum spontaneous emission rate, ignoring possible local-field corrections. See, e.g., S. Scheel, L. Knoll, D. G. Welsch, and S. M. Barnett, Phys. Rev. A **60**, 1590 (1999).
[37] In D. E. Chang, A. S. Sørensen, P. R. Hemmer, and M. D. Lukin, Phys. Rev. Lett. **97**, 053002 (2006), the maximum Purcell factor is erroneously given to be $P \sim 500$ for the nanowire, due to an error in the numerical code. This error also led to a lower predicted single-photon generation efficiency of >70% for the nanowire. All equations and discussions in that paper remain correct.
[38] W. S. Lucke, J. Appl. Phys. **22**, 14 (1951).
[39] Such an approach was used to study nanofocusing of energy in metallic tips, in M. I. Stockman, Phys. Rev. Lett. **93**, 137404 (2004).
[40] F. J. Garcia de Abajo and A. Howie, Phys. Rev. B **65**, 115418 (2002).
[41] P. Michler *et al.*, Science **290**, 2282 (2000).
[42] M. Pelton, C. Santori, J. Vuckovic, B. Zhang, G. Solomon, J. Plant, and Y. Yamamoto, Phys. Rev. Lett. **89**, 233602 (2002).
[43] J. McKeever *et al.*, Science **303**, 1992 (2004).
[44] S. J. van Enk, J. I. Cirac, and P. Zoller, Phys. Rev. Lett. **78**, 4293 (1997).
[45] J. I. Cirac, P. Zoller, H. J. Kimble, and H. Mabuchi, Phys. Rev. Lett. **78**, 3221 (1997).
[46] P. E. Barclay, K. Srinivasan, and O. Painter, J. Opt. Soc. Am. B **20**, 2274 (2003).
[47] The assumption that the field expansion in Eq. (59) can be continued all the way to the surface even in the presence of roughness is known as the Rayleigh hypothesis. See, e.g., D. Agassi and T. F. George, Phys. Rev. B **33**, 2393 (1986).
[48] T. S. Rahman and A. A. Maradudin, Phys. Rev. B **21**, 504 (1980).
[49] Y. Sun *et al.*, Nano Lett. **2**, 165 (2002).
[50] M. Barbic *et al.*, J. Appl. Phys. **91**, 9341 (2002).
[51] L. Libioulle, Y. Houbion, and J.-M. Gilles, J. Vac. Sci. Technol. B **13**, 1325 (1995).
[52] L. Tong *et al.*, Nature (London) **426**, 816 (2003).
[53] Y. A. Vlasov and S. J. McNab, Opt. Express **12**, 1622 (2004).
[54] S. A. Maier *et al.*, Appl. Phys. Lett. **84**, 3990 (2004).
[55] It can be verified that the boundary condition equations for the perpendicular field components E_ρ, H_ρ are redundant with those for the parallel field components.